

A generalized picture of colour decoherence in dense QCD media

Samuel Abreu,^{a,b} Xoán Mayo López,^c Guilherme Milhano,^{d,e} Alba Soto-Ontoso^f

^a*CERN, Theoretical Physics Department, CH-1211 Geneva 23, Switzerland*

^b*Higgs Centre for Theoretical Physics, School of Physics and Astronomy, The University of Edinburgh, Edinburgh EH9 3FD, Scotland, United Kingdom*

^c*Instituto Galego de Física de Altas Enerxías, Universidade de Santiago de Compostela, Santiago de Compostela 15782, Galicia, Spain*

^d*Laboratório de Instrumentação e Física Experimental de Partículas (LIP), Av. Prof. Gama Pinto, 2, P-1649-003 Lisboa, Portugal*

^e*Departamento de Física, Instituto Superior Técnico (IST), Universidade de Lisboa, Av. Rovisco Pais 1, P-1049-001 Lisboa, Portugal*

^f*Departamento de Física Teórica y del Cosmos, Universidad de Granada, Campus de Fuentenueva, E-18071 Granada, Spain*

ABSTRACT: We revisit the calculation of the soft gluon emission probability off a colour-singlet $q\bar{q}$ system that evolves in a quark-gluon plasma. The $q\bar{q}$ antenna is created in the presence of a medium and then emits a soft gluon outside. The gluon emission probability is modified with respect to the vacuum baseline due to interactions with the medium during the formation of the antenna and its propagation. Previous studies disregarded the former effect and found that the medium modification to the interference pattern of the antenna was controlled by the so-called critical angle θ_c , that exclusively depends on medium properties. We find that accounting for medium interactions during the antenna formation enhances the total rate of emissions off the $q\bar{q}$ antenna. Interestingly, it also promotes the notion of a critical angle to a dynamic quantity, denoted $\tilde{\theta}_c$, that depends on both the medium and the antenna properties and is thus different for every splitting. As a consequence, depending on the region of parameter space, colour decoherence can either be delayed or accelerated with respect to previous estimates.

KEYWORDS: QCD, QGP, parton branching, colour coherence

For the purpose of Open Access, the authors have applied a CC BY public copyright licence to any Author Accepted Manuscript (AAM) version arising from this submission.

Contents

1	Introduction	1
2	Amplitudes for $\gamma^* \rightarrow q\bar{q}g$ in a dense medium	4
3	$\gamma^* \rightarrow q\bar{q}g$ matrix-element in a dense medium	9
3.1	Direct terms	10
3.2	Interference term	12
3.3	Medium Modifications to Squared Matrix Elements	14
3.4	Limiting behaviour	15
4	Medium model and numerical results	16
4.1	Medium model	16
4.2	Numerical results and discussion	18
5	Conclusions	23
A	Complementary material	26

1 Introduction

Jet physics plays a key role in the characterization of the hot and dense coloured medium created in heavy-ion collisions known as the quark-gluon plasma (QGP) [1–7]. One of the most robust experimental signatures of QGP formation is the modification of the jet transverse momentum (p_t) spectrum with respect to proton-proton collisions (pp). Namely, the cross-section for producing a highly energetic jet with a given cone size R in a heavy-ion collision is suppressed [8–11], with, for instance, a 30% suppression being observed for central PbPb collisions at $p_t = 400$ GeV and $R = 0.4$ [10].

The depletion of the jet spectrum is closely related to the angular structure of the single emission matrix-element in QCD. In the absence of a medium, the probability of radiating at small angles is logarithmically enhanced because the matrix element contains a collinear singularity. In the medium, colour and momentum exchanges with the QGP, both during the formation time of the emission and its propagation, lead to a finite emission probability in the collinear limit [12–15]. Consequently, medium-induced emissions are radiated preferably at wide angles and broadened away from the emitter’s direction by subsequent interactions with the medium [16]. Some of this radiation might end up outside of the jet-cone of radius R , leading to some p_t being lost when reconstructing the jet, and thus inducing a shift in the spectrum compared to the pp result.

A natural question is whether this simple explanation for the suppression of high- p_t jets still holds when accounting for subsequent emissions. For instance, it is well known that

the angular structure of the QCD cascade in vacuum is dictated by quantum mechanical interference effects [17–20]. This can be understood at the level of two emissions by calculating the soft-gluon emission probability off a $q\bar{q}$ antenna in a colour singlet configuration. Considering the emission probability from the quark leg one finds (see e.g. [21, 22])

$$dN_q^{\text{vac}} = \frac{\alpha_s C_F}{\pi} \frac{dE_g}{E_g} \frac{\sin \theta_g d\theta_g}{1 - \cos \theta_g} \Theta(\theta_{q\bar{q}} - \theta_g), \quad (1.1)$$

where $\theta_{q\bar{q}}$ denotes the angle between the two prongs of the antenna, and θ_g the angle between the gluon and the quark. This result indicates that soft radiation at angles larger than the antenna’s opening angle is forbidden.¹ Diagrammatically, this angular structure arises from the interplay between the contributions where the gluon is emitted and reabsorbed by the (anti-)quark in the amplitude and conjugate amplitude, and those where the gluon is emitted by the quark in the amplitude and absorbed by the anti-quark in the conjugate amplitude. Thus, interference effects are responsible for the angular-ordering property of QCD radiation in vacuum, often called colour coherence.

The soft-gluon emission probability off a $q\bar{q}$ antenna including in-medium effects was computed almost 15 years ago in a series of works [23–31]. The theoretical setup considered a $q\bar{q}$ antenna that propagates through a brick of QGP with length L , emitting a soft gluon either inside or outside the medium. For simplicity, and because it already captures the main dynamical effects, we will only discuss the case in which the gluon is emitted outside. Physically, this corresponds to gluon emissions with long formation times² compared to the length of the medium, and therefore very soft. Regarding the formation of the antenna, the authors considered an instantaneous formation in the medium, which effectively sets to zero the light-cone time difference Δx_A^+ between the splitting in the amplitude and conjugate amplitude. Within this setup, the squared matrix element for gluon emission off the antenna was found to be

$$\mathcal{M}_{q\bar{q}g}^2 \sim \left(\frac{1}{\kappa^2} + \frac{1}{\bar{\kappa}^2} - 2 \frac{\kappa \cdot \bar{\kappa}}{\kappa^2 \bar{\kappa}^2} \right) + 2 \frac{\kappa \cdot \bar{\kappa}}{\kappa^2 \bar{\kappa}^2} \Delta_{\text{med}}, \quad (1.2)$$

where the first term in brackets is the vacuum result leading to the angular-ordered radiation described by Eq. (1.1), and the term proportional to Δ_{med} leads to anti-angular-ordered radiation in the complementary angular region, that is in the region corresponding to $\Theta(\theta_g - \theta_{q\bar{q}})$. The strength of this radiation is controlled by the value of Δ_{med} , the so-called ‘decoherence factor’, which accounts for medium effects and is such that $\Delta_{\text{med}} \rightarrow 0$ for vacuum and $\Delta_{\text{med}} \rightarrow 1$ for completely opaque media. Eq. (1.2) unveils a region of phase-space, controlled by medium properties, for which vacuum-like emissions at angles larger than $\theta_{q\bar{q}}$ are allowed. Thus, interference effects enable anti-angular ordered medium-induced emissions.

¹For a non-singlet configuration, Eq. (1.1) receives another contribution to the spectrum proportional to $C_A \Theta(\theta_g - \theta_{q\bar{q}})$ that can be interpreted as the large-angle gluon emissions triggered by the parent gluon.

²The concept of formation time is subtle, and we will return to it in the rest of the paper. To be more explicit here, let us denote the opening angle of a dipole as θ . The prongs have transverse momenta/energies p_{t1} and p_{t2} . Then, the vacuum formation time of an emission is given by $t_f = 2/(k_t \theta)$, with $k_t = \min(p_{t1}, p_{t2})\theta$.

The physical mechanism underlying this striking observation is called colour decoherence, and it relies on the fact that, to first approximation, the parton-medium interaction is a colour rotation. Therefore, the antenna, which starts its propagation in a colour singlet configuration, will undergo multiple interactions with the QGP which amount to colour rotations, and eventually the prongs become de-correlated in colour space. Effectively, after interacting sufficiently with the medium, the quark and anti-quark will behave as independent colour charges and the radiation phase-space is thus unconstrained. This is known as the total decoherence regime [24], and corresponds to setting $\Delta_{\text{med}} = 1$ in Eq. (1.2), canceling the interference contribution.

The previous discussion disregards the medium-modification to the antenna formation itself. Indeed, the cross-section to create an antenna is modified with respect to vacuum when allowing for a (light-cone) time gap Δx_A^+ between its formation in amplitude and conjugate amplitude [32, 33]. Owing to this interference effect, the in-medium antenna cross-section can be written as

$$\frac{d\sigma}{dz_q d\theta_{q\bar{q}}} = \frac{d\sigma^{\text{vac}}}{dz_q d\theta_{q\bar{q}}} [1 + F_{\text{med}}(E_\gamma, z_q, \theta_{q\bar{q}})], \quad (1.3)$$

where E_γ is the energy of the parent photon, z_q is the energy-sharing fraction between the antenna prongs, and $\theta_{q\bar{q}}$ the opening angle. The medium-modification factor F_{med} vanishes in the case of no medium. As one would expect, Eq. (1.3) reduces to the vacuum expression when $\Delta x_A^+ = 0$ (even though this limit is more subtle to take). This effect has been studied in Refs. [32] and [33]. The former used a semi-classical treatment, while the latter included finite N_c and finite z_q corrections. These studies have shown that F_{med} deviates from unity for a colour-singlet antenna $\gamma \rightarrow q\bar{q}$ for unbalanced splittings ($z_q \ll 0.5$) at wide angles. Interestingly, this indicates that hard-collinear splittings remain vacuum-like even in the presence of a medium, as was also pointed out in Ref. [34].

In this work, we calculate the soft-gluon emission probability off a QCD antenna in a colour singlet configuration, including both medium interference effects discussed above. That is, we account for interactions during the antenna propagation through a medium of length L while considering a non-zero Δx_A^+ . Consistently with the fact that the emitted gluon is much less energetic than the antenna legs, we focus on the case in which the emission takes place outside the medium. The main result of this paper is the squared matrix element for gluon emission off a colour singlet antenna, accounting for non-zero Δx_A^+ effects, which is given by

$$\mathcal{M}_{q\bar{q}g}^2 \sim (1 + F_{\text{med}}) \left[\left(\frac{1}{\kappa^2} + \frac{1}{\bar{\kappa}^2} - 2 \frac{\kappa \cdot \bar{\kappa}}{\kappa^2 \bar{\kappa}^2} \right) + 2 \frac{\kappa \cdot \bar{\kappa}}{\kappa^2 \bar{\kappa}^2} \tilde{\Delta}_{\text{med}} \right]. \quad (1.4)$$

The generalized decoherence factor $\tilde{\Delta}_{\text{med}}(E_\gamma, z_q, \theta_{q\bar{q}})$ is controlled by both medium and antenna properties. F_{med} is the same medium modification factor as in Eq. (1.3). In the vacuum limit, both F_{med} and $\tilde{\Delta}_{\text{med}}$ vanish and Eq. (1.4) reproduces the vacuum result. When setting $\Delta x_A^+ = 0$, Eq. (1.4) reduces to Eq. (1.2) as discussed later in the paper. Unlike Δ_{med} , $\tilde{\Delta}_{\text{med}}(E_\gamma, z_q, \theta_{q\bar{q}})$ has an intricate functional dependence on E_γ , z_q and $\theta_{q\bar{q}}$, and we find that it can be either smaller or larger than Δ_{med} , thus reducing or enhancing

the anti-angular ordered contribution. Finally, compared to Eq. (1.2) the total rate of emissions is enhanced by the F_{med} factor.

The rest of this paper is organized as follows. In Section 2 we introduce the building blocks of the calculation together with the approximations we adopted. The squared matrix element for $\gamma^* \rightarrow q\bar{q}g$ is computed in Section 3, where we also define the generalized decoherence factor $\tilde{\Delta}_{\text{med}}$. In Section 4, we present a numerical study of our results, comparing them to the Δ_{med} baseline. We conclude with some future prospects and discussion of phenomenological applications of this study in Section 5. In Appendix A we include plots to illustrate the behaviour of F_{med} , as well as a Lund plane representation of $\tilde{\Delta}_{\text{med}}$.

2 Amplitudes for $\gamma^* \rightarrow q\bar{q}g$ in a dense medium

We consider the creation and propagation of a highly boosted ultra-relativistic $q\bar{q}$ antenna in the presence of a finite, dense medium. Each prong of the antenna, with momentum p for the quark and \bar{p} for the anti-quark, is highly boosted in the z direction, that is $p_0 \sim p_z$ and similarly for \bar{p} . It is thus convenient to introduce light-cone coordinates³ such that $p = (p^+, p^-, \mathbf{p})$, where $p^+ \gg |\mathbf{p}|, p^-$. The antenna emits a gluon of momentum k , which we take to be very soft. As it has been argued in the introduction and will be explicitly seen below, this implies that its formation time is very large compared to the length of the medium, and therefore it is emitted outside of it.

Let us start by collecting the variables that we will be using throughout this paper and comment on their relative sizes. The quark and anti-quark light-cone energies are denoted E_q and $E_{\bar{q}}$ (i.e., $E_q \equiv p_+$ and $E_{\bar{q}} \equiv \bar{p}_+$), and since the gluon is very soft its energy E_g satisfies $E_g \ll E_q, E_{\bar{q}}$. The total energy is $E_\gamma = E_q + E_{\bar{q}} + E_g$. In intermediate steps, before taking the aforementioned limits, we keep explicit the sum of the quark (anti-quark) and gluon energies, which we write as

$$E_l = E_q + E_g, \quad E_{\bar{l}} = E_{\bar{q}} + E_g. \quad (2.1)$$

Finally, we introduce energy fractions which are particularly convenient for expressing our final result. We have the gluon relative energy,

$$z_g = \frac{E_g}{E_l} \sim \frac{E_g}{E_q}, \quad \bar{z}_g = \frac{E_g}{E_{\bar{l}}} \sim \frac{E_g}{E_{\bar{q}}}, \quad (2.2)$$

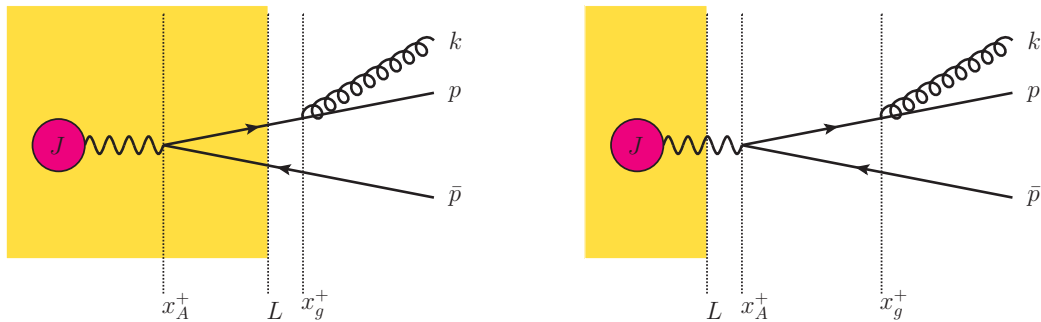
and the quark and anti-quark relative energies,

$$z_q = \frac{E_q + E_g}{E_q + E_{\bar{q}} + E_g} \sim \frac{E_q}{E_\gamma}, \quad \bar{z}_q = \frac{E_{\bar{q}} + E_g}{E_q + E_{\bar{q}} + E_g} \sim \frac{E_{\bar{q}}}{E_\gamma}. \quad (2.3)$$

These variables are not all independent since $\bar{z}_q = 1 - z_q$ and $\bar{z}_q \bar{z}_g = z_q z_g$, but introducing them is convenient to write more compact expressions.

The medium has a length $L \equiv L^+$, and it is modelled by a classical colour field, generated by static quasi-particle sources which are unaffected by interactions with the traversing

³The light-cone coordinates are defined as $v^\pm = \frac{v^0 \pm v^z}{\sqrt{2}}$, $\mathbf{v} = (v^x, v^y)$, with the dot product of two 4-vectors becoming $v \cdot w = v^+ w^- + v^- w^+ - \mathbf{v} \cdot \mathbf{w}$.



(a) **in**: Antenna formation inside the medium (b) **out**: Antenna formation outside the medium

Figure 1: Finite medium, with gluon emission outside the medium

particles. Therefore, the high-energy partons interact with a stochastic background field which can be written as

$$gA_{\text{ext}}^{a,\mu}(q) = g^{\mu+} \int_{x^+} e^{i q^- x^+} \mathcal{A}^a(x^+, \mathbf{q}) (2\pi) \delta(q^+), \quad (2.4)$$

where $g^{\mu\nu}$ is the metric tensor. $\mathcal{A}^a(x^+, \mathbf{q})$ contains the information about both the colour density of the medium scattering centres and the potential that controls the interaction between the traversing partons and the medium quasi-particles. We note that since the partons are highly boosted in the $+$ direction, the static medium sources are effectively boosted in the opposite direction and the field in Eq. (2.4) only has a non-zero component in the $-$ direction.

When computing an observable, the stochastic background field must be averaged over all possible configurations. We assume the field to have Gaussian statistics, i.e., with only pairwise averages being non-zero [35, 36]. Furthermore, we assume that interactions between the partons and the medium are local, and that there are no correlations between different sources. The average over the field configurations is then given by

$$\langle \mathcal{A}^a(x^+, \mathbf{p}) \mathcal{A}^{*b}(\bar{x}^+, \bar{\mathbf{p}}) \rangle = \frac{\delta^{ab}}{2C_{\bar{R}}} \rho(x^+) \delta(x^+ - \bar{x}^+) (2\pi)^2 \delta^{(2)}(\mathbf{p} - \bar{\mathbf{p}}) \mathcal{V}(\mathbf{p}), \quad (2.5)$$

where $\rho(x^+)$ is the number density of in-medium sources, $C_{\bar{R}} = C_A$ for quarks and $C_{\bar{R}} = C_F$ for gluons interacting with the medium, and $\mathcal{V}(\mathbf{p})$ is a screened Coulomb-like potential that controls the interaction between the traversing partons and the medium. Corrections to this simple description of the medium incorporating inhomogeneities and flow effects are the subject of an active field of research [37–46].

Given our assumption that the gluon is very soft and emitted outside the medium, there are two different amplitudes we should consider (see Fig. 1): the one where the antenna is formed inside the medium (denoted **in**), and the one where the antenna is formed outside (denoted **out**). That is, when the gluon is emitted by the quark we write

$$M_q = M_q^{\text{in}} + M_q^{\text{out}}, \quad (2.6)$$

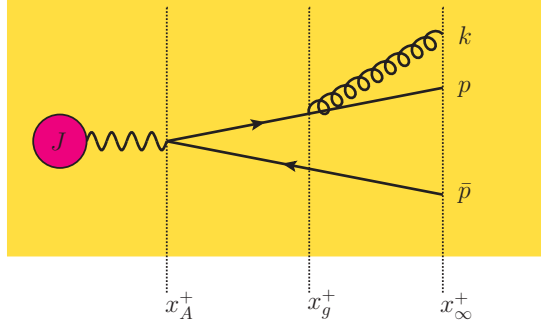


Figure 2: Antenna formation and gluon emission inside an infinite medium

and similarly for $M_{\bar{q}}$, when the gluon is emitted off the anti-quark line. For simplicity, however, we will first write the amplitude for the process where the antenna formation and the gluon emission both happen inside an infinite medium (see Fig. 2), and then take the necessary limits of this expression.

The Feynman rules describing the propagation of particles inside a medium as described above are well known and have been widely used. They can be found in e.g. Refs. [47, 48]. With these Feynman rules, the amplitude corresponding to Fig. 2 is:

$$\begin{aligned}
i M_q^{\text{med}} = & -\frac{g e}{4E_l E_\gamma} \int_0^{x_\infty^+} dx_g^+ \int_0^{x_g^+} dx_A^+ \int_{l_1, k_1, p_1, \bar{p}_1} e^{i \frac{k^2}{2E_g} x_\infty^+} \mathcal{G}^{bb_1} (x_\infty^+, \mathbf{k}; x_g^+, \mathbf{k}_1) \\
& e^{i \frac{p^2}{2E_q} x_\infty^+} \mathcal{G}_{ii_2} (x_\infty^+, \mathbf{p}; x_g^+, \mathbf{p}_1) t_{i_2 i_1}^{b_1} \gamma_{g, \lambda_g}^{\sigma_q, \sigma} [p_1; k_1] \mathcal{G}_{i_1 i_A} (x_g^+, \mathbf{p}_1 + \mathbf{k}_1; x_A^+, \mathbf{l}_1) \\
& \delta_{i_A j_A} \gamma_{A, \lambda_A}^{\sigma, \sigma_{\bar{q}}} [l_1; \bar{p}_1] \epsilon^{* \lambda_A} (l_1 + \bar{p}_1) \cdot J (l_1 + \bar{p}_1) e^{-i \frac{(l_1 + \bar{p}_1)^2}{2E_\gamma} x_a^+} \\
& e^{i \frac{\bar{p}^2}{2E_{\bar{q}}} x_\infty^+} \bar{\mathcal{G}}_{j_A j} (x_\infty^+, \bar{\mathbf{p}}; x_a^+, \bar{\mathbf{p}}_1) .
\end{aligned} \tag{2.7}$$

where $g^2 = 4\pi\alpha_s$ and e is the electric charge. Let us make some comments on this expression. The propagation of each particle inside the medium is described by an in-medium propagator, \mathcal{G} , which allows for colour rotations and transverse motion as particles advance through the matter. In our approximation, the spinor index or helicity of the particles is not modified by medium interactions. The external spinors and polarisations are absorbed into the definition of the medium propagators, and the vertices include the spinors and helicities at the interaction point. More explicitly, the vertices are

$$\begin{aligned}
\gamma_{A, \lambda_A}^{\sigma, \sigma_{\bar{q}}} [l_1; \bar{p}_1] &= \bar{u}^\sigma (l_1) \not{\epsilon}^{\lambda_A} (l_1 + \bar{p}_1) v^{\sigma_{\bar{q}}} (\bar{p}_1) , \\
\gamma_{g, \lambda_g}^{\sigma_q, \sigma} [p_1; k_1] &= \bar{u}^{\sigma_q} (p_1) \not{\epsilon}^{* \lambda_g} (k_1) u^\sigma (p_1 + k_1) ,
\end{aligned} \tag{2.8}$$

where σ_q and $\sigma_{\bar{q}}$ are the spinor indices of the external quark and anti-quark, and λ_g the polarisation of the external gluon. The current J^μ describes the creation of the virtual photon. Note that these expressions only depend on the energy and transverse components of each of the momenta, since the minus component has been integrated out introducing

the dependence on the light-cone time, but for simplicity of the notation we write them as depending on the full four-momenta. Finally, in Eq. (2.7) there is a phase associated with each external propagator, as well as the one corresponding to the vacuum propagator of the photon.

Given that the prongs of the antenna are very energetic, we assume that they propagate along straight lines and we write the quark propagators as (tilted) eikonal propagators. Thus, the description of highly unbalanced splittings, with z_q very close to 0 or 1, is beyond the regime of validity of our approximation. Following Refs. [32, 49], if we further set the initial position of the eikonal propagators in the transverse plane to zero, then we have that

$$\mathcal{G}_{ij}^{\text{eik}}(x_2^+, \mathbf{p}_2; x_1^+, \mathbf{p}_1) = (2\pi)^2 \delta^{(2)}(\mathbf{p}_2 - \mathbf{p}_1) e^{-i \frac{\mathbf{p}_2^2}{2E}(x_2^+ - x_1^+)} \mathcal{W}_{ij}(x_2^+, x_1^+; \frac{\mathbf{p}_2}{E}(\tau - x_1^+)) , \quad (2.9)$$

and similarly for the anti-quark. Replacing the propagators in Eq. (2.7) by eikonal propagators already leads to a considerable simplification that allows us to perform some of the integrations over transverse components in the amplitude. To further simplify it, we focus on the limits corresponding to Fig. 1. We start with the **in** case of Fig. 1a. Taking the amplitude in Eq. (2.7) as our starting point, we note that the emitted gluon is outside the medium, so its propagator becomes a free propagator,

$$\mathcal{G}^{bb_1}(x_\infty^+, \mathbf{k}; x_g^+, \mathbf{k}_1) \rightarrow \delta_{bb_1} (2\pi)^2 \delta^{(2)}(\mathbf{k}_1 - \mathbf{k}) e^{-i \frac{\mathbf{k}^2}{2E_g}(x_\infty^+ - x_g^+)} . \quad (2.10)$$

Combined with the replacement of the quark and anti-quark propagators with eikonal propagators, this allows us to perform all the transverse momentum integrals. We also note that after these replacements the dependence on x_∞^+ in the phases cancels out. Finally, we note that the Wilson lines in the quark and anti-quark eikonal propagators either simplify or become ‘shorter’. Explicitly,

$$\begin{aligned} \mathcal{W}_{ii_2}(x_\infty^+, x_g^+; \frac{\mathbf{p}}{E_q}(\tau - x_g^+)) &\rightarrow \delta_{ii_2} , \\ \mathcal{W}_{i_1 i_A}(x_g^+, x_A^+; \frac{\mathbf{p} + \mathbf{k}}{E_q + E_g}(\tau - x_g^+)) &\rightarrow \mathcal{W}_{i_1 i_A}(L, x_A^+; \mathbf{r}_q^A(\tau)) , \\ \mathcal{W}_{j_A j}^\dagger(x_g^+, x_A^+; \frac{\bar{\mathbf{p}}}{E_{\bar{q}}}(\tau - x_g^+)) &\rightarrow \mathcal{W}_{j_A j}^\dagger(L, x_A^+; \mathbf{r}_{\bar{q}}^A(\tau)) , \end{aligned} \quad (2.11)$$

where for the quark line we also neglected the gluon momentum compared to the much harder quark momentum, and we have defined the trajectories

$$\mathbf{r}_q^A(\tau) = \frac{\mathbf{p}}{E_q}(\tau - x_A^+) , \quad \mathbf{r}_{\bar{q}}^A(\tau) = \frac{\bar{\mathbf{p}}}{E_{\bar{q}}}(\tau - x_A^+) . \quad (2.12)$$

With these simplifications and assumptions, the momenta at each vertex become the external momenta of the quark, anti-quark and gluon.

Finally, we obtain the amplitude corresponding to the diagram in Fig. 1a:

$$\begin{aligned} i M_q^{\text{in}} &= - \frac{g e}{4E_l E_\gamma} \int_L^{x_\infty^+} dx_g^+ e^{i \frac{x_g^+}{t_g}} \int_0^L dx_A^+ e^{i \frac{x_A^+}{t_A}} t_{ii_1}^b \mathcal{W}_{i_1 i_A}(L, x_A^+; \mathbf{r}_q^A(\tau)) \\ &\times \mathcal{W}_{i_A j}^\dagger(L, x_A^+; \mathbf{r}_{\bar{q}}^A(\tau)) \gamma_{g, \lambda_g}^{\sigma_q, \sigma} [p; k] \gamma_{A, \lambda_A}^{\sigma, \sigma_{\bar{q}}} [p; \bar{p}] \epsilon^{*\lambda_A} (p + \bar{p}) \cdot J(p + \bar{p}) , \end{aligned} \quad (2.13)$$

where we took the limit of a soft gluon and we introduced the formation times for the gluon and the antenna,

$$t_g = \frac{2z_g z_q E_\gamma}{(\mathbf{k} - z_g \mathbf{p})^2}, \quad t_A = \frac{2z_q(1-z_q)E_\gamma}{[(1-z_q)\mathbf{p} - z_q \bar{\mathbf{p}}]^2}. \quad (2.14)$$

As argued previously, it is clear that for a very soft gluon (i.e., $z_g, |\mathbf{k}| \rightarrow 0$) the gluon formation time is very large.

Given that in the diagram of Fig. 1a the point x_g^+ is an arbitrary point in vacuum, we would expect to be able to trivially integrate it, and this is indeed the case in Eq. (2.13) as it only appears in a phase. The contribution of this integral at x_∞^+ vanishes, while the contribution at the other limit of integration gives a phase e^{iL/t_g} , which we can set to 1 because $t_g \gg L$ for a very soft gluon. We then find

$$i M_q^{\text{in}} = -\frac{i g e t_g}{4E_l E_\gamma} \int_0^L dx_A^+ e^{i \frac{x_A^+}{t_A} t_{ii_1}^b} \mathcal{W}_{i_1 i_A} (L, x_A^+; \mathbf{r}_q^A(\tau)) \mathcal{W}_{i_A j}^\dagger (L, x_A^+; \mathbf{r}_{\bar{q}}^A(\tau)) \gamma_{g, \lambda_g}^{\sigma_q, \sigma} [p; k] \gamma_{A, \lambda_A}^{\sigma, \sigma_{\bar{q}}} [p; \bar{p}] \epsilon^{*\lambda_A} (p + \bar{p}) \cdot J (p + \bar{p}). \quad (2.15)$$

The **out** case, corresponding to Fig. 1b, is trivial to obtain following exactly the same steps. We get

$$i M_q^{\text{out}} = -\frac{g e}{4E_l E_\gamma} \int_L^{x_\infty^+} dx_g^+ e^{i \frac{x_g^+}{t_g}} \int_L^{x_g^+} dx_A^+ e^{i \frac{x_A^+}{t_A}} t_{ij}^b \gamma_{g, \lambda_g}^{\sigma_q, \sigma} [p; k] \gamma_{A, \lambda_A}^{\sigma, \sigma_{\bar{q}}} [p; \bar{p}] \epsilon^{*\lambda_A} (p + \bar{p}) \cdot J (p + \bar{p}). \quad (2.16)$$

Noticing that both the x_g^+ and x_A^+ dependences can be integrated trivially we find

$$i M_q^{\text{out}} = \frac{g e}{4E_l E_\gamma} t_A t_g e^{i \frac{L}{t_A}} t_{ij}^b \gamma_{g, \lambda_g}^{\sigma_q, \sigma} [p; k] \gamma_{A, \lambda_A}^{\sigma, \sigma_{\bar{q}}} [p; \bar{p}] \epsilon^{*\lambda_A} (p + \bar{p}) \cdot J (p + \bar{p}), \quad (2.17)$$

where we have again used that $t_g \gg L$.

The amplitudes corresponding to emissions off the anti-quark leg can be obtained in exactly the same way. We get:

$$i M_{\bar{q}}^{\text{in}} = \frac{i g e \bar{t}_g}{4E_{\bar{l}} E_\gamma} \int_0^L dx_A^+ e^{i \frac{x_A^+}{t_A}} \mathcal{W}_{i i_A} (L, x_A^+; \mathbf{r}_q^A(\tau)) \mathcal{W}_{i_A j_1}^\dagger (L, x_A^+; \mathbf{r}_{\bar{q}}^A(\tau)) t_{j_1 j}^b \bar{\gamma}_{g, \lambda_g}^{\sigma, \sigma_{\bar{q}}} [\bar{p}; k] \gamma_{A, \lambda_A}^{\sigma_q, \sigma} [p; \bar{p}] \epsilon^{*\lambda_A} (p + \bar{p}) \cdot J (p + \bar{p}), \quad (2.18)$$

and

$$i M_{\bar{q}}^{\text{out}} = -\frac{g e}{4E_{\bar{l}} E_\gamma} t_A \bar{t}_g e^{i \frac{L}{t_A}} t_{ij}^b \bar{\gamma}_{g, \lambda_g}^{\sigma, \sigma_{\bar{q}}} [\bar{p}; k] \gamma_{A, \lambda_A}^{\sigma_q, \sigma} [p; \bar{p}] \epsilon^{*\lambda_A} (p + \bar{p}) \cdot J (p + \bar{p}). \quad (2.19)$$

These expressions depend on the gluon formation time when it is radiated off the \bar{q} line,

$$\bar{t}_g = \frac{2\bar{z}_g(1-\bar{z}_q)E_\gamma}{(\mathbf{k} - \bar{z}_g \bar{\mathbf{p}})^2}, \quad (2.20)$$

and on the corresponding vertex

$$\bar{\gamma}_{g, \lambda_g}^{\sigma, \sigma_{\bar{q}}} [\bar{p}; k] = \bar{v}^\sigma (\bar{p} + k) \not{\epsilon}^{*\lambda_g} (k) v^{\sigma_{\bar{q}}} (\bar{p}). \quad (2.21)$$

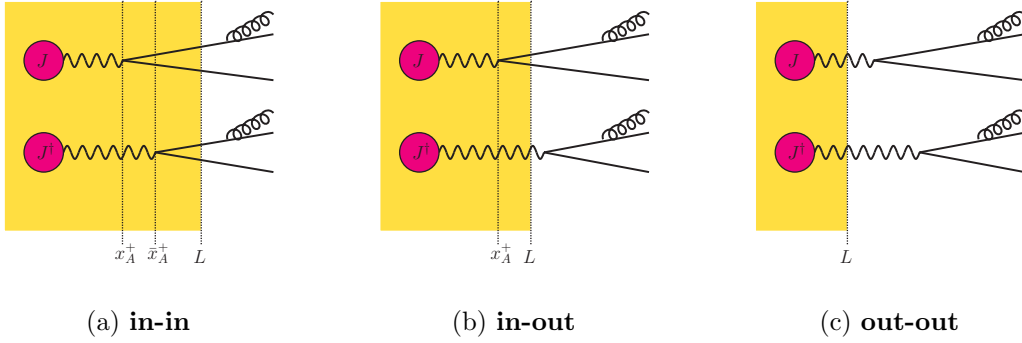


Figure 3: Different contributions to Eq. (3.2). The amplitude is depicted on top of the corresponding conjugate amplitude. For the **in-out** contributions we omit the diagram where the roles of the amplitude and conjugate amplitude are reversed.

3 $\gamma^* \rightarrow q\bar{q}g$ matrix-element in a dense medium

Equipped with the M_q and $M_{\bar{q}}$ amplitudes derived in the previous section, we can now calculate the squared matrix element $\mathcal{M}_{q\bar{q}g}^2$ for $\gamma^* \rightarrow q\bar{q}g$ splittings,

$$\mathcal{M}_{q\bar{q}g}^2 = \langle |M_q|^2 \rangle + \langle |M_{\bar{q}}|^2 \rangle + \langle 2 \operatorname{Re} M_q M_{\bar{q}}^* \rangle, \quad (3.1)$$

where the product of amplitudes has also been averaged over medium configurations, and the standard average over initial and sum over final quantum numbers is implicit. We refer to the first two contributions in Eq. (3.1) as *direct terms*, since they correspond to the gluon being emitted by either the quark or the anti-quark both in the amplitude and the conjugate amplitude. The last contribution is referred to as the *interference term*.

Each of the contributions in Eq. (3.1) can be written as the sum over three regions depending on the light-cone time of the antenna formation, see Fig. 3: the **in-in** region, where the antenna is created inside the medium in amplitude and conjugate amplitude; the **in-out** region, where one of the antennas is created inside and the other one outside the medium; and the **out-out** region, where both are created once the photon has escaped the medium. For instance, given the decomposition in Eq. (2.6), we will compute $|M_q|^2$ as the sum of

$$\begin{aligned} |M_q|_{\text{in-in}}^2 &= M_q^{\text{in}} M_q^{\text{in},\dagger}, & |M_q|_{\text{in-out}}^2 &= M_q^{\text{in}} M_q^{\text{out},\dagger} + M_q^{\text{out}} M_q^{\text{in},\dagger}, \\ |M_q|_{\text{out-out}}^2 &= M_q^{\text{out}} M_q^{\text{out},\dagger}. \end{aligned} \quad (3.2)$$

In the various terms above we need to sum and average over the corresponding quantum numbers. This procedure affects both the product of the polarization vectors and the vertices given in Eqs. (2.8) and (2.21). The former simply becomes

$$\epsilon^{\lambda A}(p + \bar{p}) \cdot J(p + \bar{p}) \left(\epsilon^{\bar{\lambda} A}(p + \bar{p}) \cdot J(p + \bar{p}) \right)^\dagger \rightarrow \delta^{\lambda A \bar{\lambda} A} |J(p + \bar{p})|^2. \quad (3.3)$$

The latter, including the average over the photon polarization corresponding to the factor 1/2 below, give

$$\begin{aligned} \frac{1}{2} \sum \gamma_{A,\lambda_A}^{\sigma_q,\sigma} [p; \bar{p}] \bar{\gamma}_{g,\lambda_g}^{\sigma,\sigma_{\bar{q}}} [\bar{p}; k] \left[\gamma_{A,\lambda_A}^{\sigma_q,\bar{\sigma}} [p; \bar{p}] \bar{\gamma}_{g,\lambda_g}^{\bar{\sigma},\sigma_{\bar{q}}} [\bar{p}; k] \right]^* &= \frac{32E_\gamma^2 z_q}{t_A t_g z_g} P_{\gamma \rightarrow q\bar{q}}(z_q), \\ \frac{1}{2} \sum \gamma_{g,\lambda_g}^{\sigma_q,\sigma} [p; k] \gamma_{A,\lambda_A}^{\sigma,\sigma_{\bar{q}}} [p; \bar{p}] \left[\gamma_{A,\lambda_A}^{\sigma_q,\bar{\sigma}} [p; \bar{p}] \bar{\gamma}_{g,\lambda_g}^{\bar{\sigma},\sigma_{\bar{q}}} [\bar{p}; k] \right]^* &= \boldsymbol{\kappa} \cdot \bar{\boldsymbol{\kappa}} \frac{16E_\gamma}{\bar{z}_g z_g t_A} P_{\gamma \rightarrow q\bar{q}}(z_q), \end{aligned} \quad (3.4)$$

where $P_{\gamma \rightarrow q\bar{q}}(z_q) = n_f [z_q^2 + (1 - z_q)^2]$ is the vacuum splitting function, and we have introduced

$$\boldsymbol{\kappa} = \mathbf{k} - z_g \mathbf{p}, \quad \bar{\boldsymbol{\kappa}} = \mathbf{k} - \bar{z}_g \bar{\mathbf{p}} \quad (3.5)$$

i.e., the relative transverse momentum of the gluon with respect to the quark and the anti-quark respectively.

3.1 Direct terms

In-in region: After summing and averaging over quantum numbers, the squared amplitude is given by

$$\begin{aligned} \sum |M_q|_{\text{in-in}}^2 &= 2 \text{Re} C_F \left(\frac{g e}{E_\gamma} \right)^2 \frac{2t_g}{z_q t_A} \frac{1}{z_g} P_{\gamma \rightarrow q\bar{q}}(z_q) |J(p + \bar{p})|^2 \\ &\times \int_0^L d\bar{x}_A^+ \int_0^{\bar{x}_A^+} dx_A^+ e^{-i \frac{\Delta x_A^+}{t_A}} \mathcal{W}_{kl}(L, x_A^+; \mathbf{r}_q^A(\tau)) \mathcal{W}_{li}^\dagger(L, x_A^+; \mathbf{r}_{\bar{q}}^A(\tau)) \\ &\times \mathcal{W}_{i\bar{l}}(L, \bar{x}_A^+; \bar{\mathbf{r}}_{\bar{q}}^A(\tau)) \mathcal{W}_{\bar{l}k}^\dagger(L, \bar{x}_A^+; \bar{\mathbf{r}}_q^A(\tau)), \end{aligned} \quad (3.6)$$

where the trajectory of the Wilson lines in the amplitude is parametrized as in Eq. (2.12) and in the conjugate amplitude by

$$\bar{\mathbf{r}}_q^A(\tau) = \frac{\mathbf{p}}{E_q} (\tau - \bar{x}_A^+), \quad \bar{\mathbf{r}}_{\bar{q}}^A(\tau) = \frac{\bar{\mathbf{p}}}{E_{\bar{q}}} (\tau - \bar{x}_A^+). \quad (3.7)$$

We have chosen $\Delta x_A^+ = \bar{x}_A^+ - x_A^+ > 0$, accounting for the alternative ordering by taking twice the real part of the expression. The Casimir of the fundamental representation appears through $t_{\bar{k}j}^b t_{jk}^b = C_F \delta_{\bar{k}k}$.

The next step is to average $|M_q|^2$ over medium configurations. Given that the medium average is local in the + component (see Eq. (2.4)), we use the composition law of Wilson lines

$$\mathcal{W}_{ab}(x_1^+, x_2^+; \mathbf{r}(\tau)) = \mathcal{W}_{ac}(x_1^+, x_3^+; \mathbf{r}(\tau)) \mathcal{W}_{cb}(x_3^+, x_2^+; \mathbf{r}(\tau)) \quad (3.8)$$

to rewrite the squared amplitude as

$$\begin{aligned} \sum \langle |M_q|_{\text{in-in}}^2 \rangle &= 2 \text{Re} C_F \left(\frac{g e}{E_\gamma} \right)^2 \frac{2t_g}{z_q t_A} \frac{1}{z_g} P_{\gamma \rightarrow q\bar{q}}(z_q) |J(p + \bar{p})|^2 \\ &\times \int_0^L d\bar{x}_A^+ \int_0^{\bar{x}_A^+} dx_A^+ e^{-i \frac{\Delta x_A^+}{t_A}} \left\langle \mathcal{W}_{ml}(\bar{x}_A^+, x_A^+; \mathbf{r}_q^A(\tau)) \mathcal{W}_{ln}^\dagger(\bar{x}_A^+, x_A^+; \mathbf{r}_{\bar{q}}^A(\tau)) \right\rangle \\ &\times \left\langle \mathcal{W}_{km}(L, \bar{x}_A^+; \mathbf{r}_q^A(\tau)) \mathcal{W}_{ni}^\dagger(L, \bar{x}_A^+; \mathbf{r}_{\bar{q}}^A(\tau)) \mathcal{W}_{i\bar{l}}(L, \bar{x}_A^+; \bar{\mathbf{r}}_{\bar{q}}^A(\tau)) \mathcal{W}_{\bar{l}k}^\dagger(L, \bar{x}_A^+; \bar{\mathbf{r}}_q^A(\tau)) \right\rangle. \end{aligned} \quad (3.9)$$

Then, we also use the property of colour triviality (see Eq. (2.5)) to obtain

$$\begin{aligned} & \left\langle \mathcal{W}_{ml}(\bar{x}_A^+, x_A^+; \mathbf{r}_q^A(\tau)) \mathcal{W}_{ln}^\dagger(\bar{x}_A^+, x_A^+; \mathbf{r}_{\bar{q}}^A(\tau)) \right\rangle \\ &= \frac{\delta_{mn}}{N_c} \left\langle \text{Tr} \mathcal{W}(\bar{x}_A^+, x_A^+; \mathbf{r}_q^A(\tau)) \mathcal{W}^\dagger(\bar{x}_A^+, x_A^+; \mathbf{r}_{\bar{q}}^A(\tau)) \right\rangle, \end{aligned} \quad (3.10)$$

and similarly for the medium average of four Wilson lines. Putting everything together we get our final expression for the **in-in** contribution to the direct term

$$\begin{aligned} \sum \langle |M_q|_{\text{in-in}}^2 \rangle &= 4 C_F N_c \left(\frac{g e}{E_\gamma} \right)^2 \frac{t_g}{z_q t_A} \frac{1}{z_g} P_{\gamma \rightarrow q\bar{q}}(z_q) |J(p + \bar{p})|^2 \\ &\times \int_0^L d\bar{x}_A^+ \int_0^{\bar{x}_A^+} dx_A^+ \cos\left(\frac{\Delta x_A^+}{t_A}\right) \mathcal{S}^{(2)}(\bar{x}_A^+, x_A^+; \mathbf{r}_q^A(\tau), \mathbf{r}_{\bar{q}}^A(\tau)) \\ &\times \mathcal{Q}^{(4)}(L, \bar{x}_A^+; \mathbf{r}_q^A(\tau), \mathbf{r}_{\bar{q}}^A(\tau), \bar{\mathbf{r}}_q^A(\tau), \bar{\mathbf{r}}_{\bar{q}}^A(\tau)). \end{aligned} \quad (3.11)$$

We have introduced the two-point function $\mathcal{S}^{(2)}$, usually referred to as ‘dipole’ in the literature,

$$\mathcal{S}^{(2)}(\bar{x}_A^+, x_A^+; \mathbf{r}_q^A(\tau), \mathbf{r}_{\bar{q}}^A(\tau)) = \frac{1}{N_c} \left\langle \text{Tr} \mathcal{W}(\bar{x}_A^+, x_A^+; \mathbf{r}_q^A(\tau)) \mathcal{W}^\dagger(\bar{x}_A^+, x_A^+; \mathbf{r}_{\bar{q}}^A(\tau)) \right\rangle, \quad (3.12)$$

and the four-point function $\mathcal{Q}^{(4)}$, the so-called ‘quadrupole’,

$$\begin{aligned} & \mathcal{Q}^{(4)}(L, \bar{x}_A^+; \mathbf{r}_q^A(\tau), \mathbf{r}_{\bar{q}}^A(\tau), \bar{\mathbf{r}}_q^A(\tau), \bar{\mathbf{r}}_{\bar{q}}^A(\tau)) \\ &= \frac{1}{N_c} \left\langle \text{Tr} \mathcal{W}(L, \bar{x}_A^+; \mathbf{r}_q^A(\tau)) \mathcal{W}^\dagger(L, \bar{x}_A^+; \mathbf{r}_{\bar{q}}^A(\tau)) \mathcal{W}(L, \bar{x}_A^+; \bar{\mathbf{r}}_q^A(\tau)) \mathcal{W}^\dagger(L, \bar{x}_A^+; \bar{\mathbf{r}}_{\bar{q}}^A(\tau)) \right\rangle. \end{aligned} \quad (3.13)$$

Both the dipole and the quadrupole are purely real functions.

In the first line of Eq. (3.11) we recognise the vacuum splitting function for the gluon emission in the soft limit $P_{q \rightarrow qg} = 1/z_g$. This observation renders a clear separation between the gluon emission process and the medium dynamics, as expected given the limits we have taken throughout our calculation.

In-out region: We next turn to the case in which the antenna is created outside the medium either in the amplitude or in the conjugate amplitude. We find that the squared amplitude is given by

$$\begin{aligned} \sum |M_q|_{\text{in-out}}^2 &= 2i C_F \left(\frac{g e}{E_\gamma} \right)^2 \frac{t_g}{z_q z_g} P_{\gamma \rightarrow q\bar{q}}(z_q) |J(p + \bar{p})|^2 \\ &\times \left\{ \int_0^L dx_A^+ e^{i \frac{(L-x_A^+)}{t_A}} \mathcal{W}_{il}(L, x_A^+; \mathbf{r}_q^A(\tau)) \mathcal{W}_{li}^\dagger(L, x_A^+; \mathbf{r}_{\bar{q}}^A(\tau)) \right. \\ &\quad \left. - \int_0^L dx_A^+ e^{-i \frac{(L-x_A^+)}{t_A}} \mathcal{W}_{il}(L, x_A^+; \mathbf{r}_{\bar{q}}^A(\tau)) \mathcal{W}_{li}^\dagger(L, x_A^+; \mathbf{r}_q^A(\tau)) \right\}. \end{aligned} \quad (3.14)$$

Note that after performing the medium average, the two terms in the curly brackets are identical up to the sign in the phase. Therefore, we obtain

$$\begin{aligned} \sum \langle |M_q|_{\text{in-out}}^2 \rangle &= -4 C_F N_c \left(\frac{g e}{E_\gamma} \right)^2 \frac{t_g}{z_g z_q} P_{\gamma \rightarrow q\bar{q}}(z_q) |J(p + \bar{p})|^2 \\ &\times \int_0^L dx_A^+ \sin \left(\frac{L - x_A^+}{t_A} \right) \mathcal{S}^{(2)}(L, x_A^+; \mathbf{r}_q^A(\tau), \mathbf{r}_{\bar{q}}^A(\tau)), \end{aligned} \quad (3.15)$$

where we have introduced the dipole as defined in Eq. (3.12).

Out-out region: Lastly, we study the case in which the antenna is formed outside the medium. All Wilson lines become Kronecker deltas in colour space, and all integrals can be trivially computed to get

$$\sum \langle |M_q|_{\text{out-out}}^2 \rangle = 2 C_F N_c \left(\frac{g e}{E_\gamma} \right)^2 \frac{t_g t_A}{z_q z_g} P_{\gamma \rightarrow q\bar{q}}(z_q) |J(p + \bar{p})|^2, \quad (3.16)$$

which coincides with the direct quark contribution to the squared matrix element for gluon radiation from a colour singlet antenna in vacuum.

The full result for the direct quark contributions is obtained by summing Eqs. (3.11), (3.15) and (3.16). The direct anti-quark contributions can be obtained from the quark results by replacing $z_g \rightarrow \bar{z}_g$, $z_q \rightarrow \bar{z}_q = (1 - z_q)$ and $t_g \rightarrow \bar{t}_g$.

3.2 Interference term

Here we compute the contribution to the squared matrix element in which the radiation is emitted from one leg of the antenna in the amplitude, and absorbed by the other one in the conjugated amplitude. These diagrams are responsible for interference effects between the gluon emission and the dynamics of the antenna formation, as we shall discuss in more detail below.

In-in region: We start by focusing on the region where the antenna is created inside the medium. The squared matrix element is given by

$$\begin{aligned} 2 \text{Re} \sum (M_q M_{\bar{q}}^*)_{\text{in-in}} &= -2 \text{Re} \frac{(g e)^2}{z_q (1 - z_q) E_\gamma^3} \frac{t_g \bar{t}_g}{\bar{z}_g z_g t_A} |J(p + \bar{p})|^2 \boldsymbol{\kappa} \cdot \bar{\boldsymbol{\kappa}} P_{\gamma \rightarrow q\bar{q}}(z_q) \\ &\times \int_0^L d\bar{x}_A^+ \int_0^{\bar{x}_A^+} dx_A^+ \left[e^{-i \frac{\Delta x_A^+}{t_A}} t_{jk}^b \mathcal{W}_{kl}(L, x_A^+; \mathbf{r}_q^A(\tau)) \mathcal{W}_{li}^\dagger(L, x_A^+; \mathbf{r}_{\bar{q}}^A(\tau)) \right. \\ &\times \left. t_{i\bar{k}}^b \mathcal{W}_{\bar{k}\bar{l}}(L, \bar{x}_A^+; \bar{\mathbf{r}}_{\bar{q}}^A(\tau)) \mathcal{W}_{l\bar{j}}^\dagger(L, \bar{x}_A^+; \bar{\mathbf{r}}_q^A(\tau)) + (x_A^+ \leftrightarrow \bar{x}_A^+) \right], \end{aligned} \quad (3.17)$$

where we accounted for the two possible orderings of the light-cone times of the antenna splitting. Let us comment on the colour structure. By using the Fierz identity we can rewrite the product of $SU(N_c)$ generators as

$$t_{jk}^b t_{i\bar{k}}^b = \frac{1}{2} \left(\delta_{j\bar{k}} \delta_{ki} - \frac{1}{N_c} \delta_{jk} \delta_{i\bar{k}} \right). \quad (3.18)$$

The first term of the previous equation, when combined with the colour structure of the Wilson lines, leads to

$$\begin{aligned}
2 \operatorname{Re} \sum (M_q M_q^*)_{\mathbf{in-in}} &= -\operatorname{Re} \frac{(ge)^2}{z_q(1-z_q)E_\gamma^3} \frac{t_g \bar{t}_g}{\bar{z}_g z_g t_A} |J(p+\bar{p})|^2 \boldsymbol{\kappa} \cdot \bar{\boldsymbol{\kappa}} P_{\gamma \rightarrow q\bar{q}}(z_q) \\
&\times \int_0^L d\bar{x}_A^+ \int_0^{\bar{x}_A^+} dx_A^+ \left[e^{-i \frac{\Delta x_A^+}{t_A}} \mathcal{W}_{kl}(L, x_A^+; \mathbf{r}_q^A(\tau)) \mathcal{W}_{lk}^\dagger(L, x_A^+; \mathbf{r}_{\bar{q}}^A(\tau)) \right. \\
&\times \left. \mathcal{W}_{j\bar{l}}(L, \bar{x}_A^+; \bar{\mathbf{r}}_{\bar{q}}^A(\tau)) \mathcal{W}_{l\bar{j}}^\dagger(L, \bar{x}_A^+; \bar{\mathbf{r}}_q^A(\tau)) + (x_A^+ \leftrightarrow \bar{x}_A^+) \right]. \tag{3.19}
\end{aligned}$$

We neglect the contribution arising from the second term in the Fierz identity since we work in the large- N_c limit.

Averaging Eq. (3.19) over all possible configurations of the background field and using their locality and colour triviality leads to

$$\begin{aligned}
2 \operatorname{Re} \sum \langle M_q M_q^* \rangle_{\mathbf{in-in}} &= -4 \operatorname{Re} C_F N_c \frac{(ge)^2}{z_q(1-z_q)E_\gamma^3} \frac{t_g \bar{t}_g}{\bar{z}_g z_g t_A} |J(p+\bar{p})|^2 \boldsymbol{\kappa} \cdot \bar{\boldsymbol{\kappa}} P_{\gamma \rightarrow q\bar{q}}(z_q) \\
&\times \int_0^L d\bar{x}_A^+ \int_0^{\bar{x}_A^+} dx_A^+ \left[e^{-i \frac{\Delta x_A^+}{t_A}} \frac{1}{N_c} \left\langle \mathcal{W}_{ml}(\bar{x}_A^+, x_A^+; \mathbf{r}_q^A(\tau)) \mathcal{W}_{lm}^\dagger(\bar{x}_A^+, x_A^+; \mathbf{r}_{\bar{q}}^A(\tau)) \right\rangle \right. \\
&\times \left. \frac{1}{N_c^2} \left\langle \mathcal{W}_{in}(L, \bar{x}_A^+; \mathbf{r}_q^A(\tau)) \mathcal{W}_{ni}^\dagger(L, \bar{x}_A^+; \mathbf{r}_{\bar{q}}^A(\tau)) \mathcal{W}_{j\bar{l}}(L, \bar{x}_A^+; \bar{\mathbf{r}}_{\bar{q}}^A(\tau)) \mathcal{W}_{l\bar{j}}^\dagger(L, \bar{x}_A^+; \bar{\mathbf{r}}_q^A(\tau)) \right\rangle \right], \tag{3.20}
\end{aligned}$$

where the overall factor of 4 comes from writing $N_c^2 = 2C_F N_c$ in the large- N_c limit and taking into account the two orderings of the integration variables written explicitly in Eq. (3.19). We identify two structures of Wilson-line correlators: a dipole between x_A^+ and \bar{x}_A^+ , $\mathcal{S}^{(2)}(\bar{x}_A^+, x_A^+; \mathbf{r}_q^A(\tau), \mathbf{r}_{\bar{q}}^A(\tau))$ (see Eq. (3.12)), and the product of four Wilson lines that are traced into two pairs, the so-called ‘double-dipole’. In the large- N_c limit, it can be shown that this object reduces to the product of two dipoles (see e.g. Ref. [50]). Therefore, we can further simplify Eq. (3.20) and obtain

$$\begin{aligned}
2 \operatorname{Re} \sum \langle M_q M_q^* \rangle_{\mathbf{in-in}} &= -4 C_F N_c \frac{(ge)^2}{z_q(1-z_q)E_\gamma^3} \frac{t_g \bar{t}_g}{\bar{z}_g z_g t_A} |J(p+\bar{p})|^2 \boldsymbol{\kappa} \cdot \bar{\boldsymbol{\kappa}} P_{\gamma \rightarrow q\bar{q}}(z_q) \\
&\times \int_0^L d\bar{x}_A^+ \int_0^{\bar{x}_A^+} dx_A^+ \cos\left(\frac{\Delta x_A^+}{t_A}\right) \mathcal{S}^{(2)}(\bar{x}_A^+, x_A^+; \mathbf{r}_q^A(\tau), \mathbf{r}_{\bar{q}}^A(\tau)) \\
&\times \mathcal{S}^{(2)}(L, \bar{x}_A^+; \mathbf{r}_q^A(\tau), \mathbf{r}_{\bar{q}}^A(\tau)) \mathcal{S}^{(2)}(L, \bar{x}_A^+; \bar{\mathbf{r}}_{\bar{q}}^A(\tau), \bar{\mathbf{r}}_q^A(\tau)). \tag{3.21}
\end{aligned}$$

In-out region: The colour structure heavily simplifies in this situation since, analogously to the direct term calculation, we have to deal with only two Wilson lines. The result is

$$\begin{aligned}
2 \operatorname{Re} \sum (M_q M_q^*)_{\mathbf{in-out}} &= 2i \operatorname{Re} C_F \frac{(ge)^2}{z_q(1-z_q)E_\gamma^3} \frac{t_g \bar{t}_g}{\bar{z}_g z_g} |J(p+\bar{p})|^2 \boldsymbol{\kappa} \cdot \bar{\boldsymbol{\kappa}} P_{\gamma \rightarrow q\bar{q}}(z_q) \\
&\times \left\{ \int_0^L dx_A^+ e^{-i \frac{(L-x_A^+)}{t_A}} \mathcal{W}_{il}(L, x_A^+; \mathbf{r}_q^A(\tau)) \mathcal{W}_{li}^\dagger(L, x_A^+; \mathbf{r}_{\bar{q}}^A(\tau)) \right. \\
&\left. - \int_0^L dx_A^+ e^{i \frac{(L-x_A^+)}{t_A}} \mathcal{W}_{li}(L, x_A^+; \mathbf{r}_{\bar{q}}^A(\tau)) \mathcal{W}_{il}^\dagger(L, x_A^+; \mathbf{r}_q^A(\tau)) \right\}. \tag{3.22}
\end{aligned}$$

After performing the medium average, this expression reduces to

$$2 \operatorname{Re} \sum \langle M_q M_{\bar{q}}^* \rangle_{\text{in-out}} = 4 C_F N_c \frac{(ge)^2}{z_q(1-z_q)E_\gamma^3} \frac{t_g \bar{t}_g}{\bar{z}_g z_g} |J(p+\bar{p})|^2 \boldsymbol{\kappa} \cdot \bar{\boldsymbol{\kappa}} P_{\gamma \rightarrow q\bar{q}}(z_q) \quad (3.23)$$

$$\times \int_0^L dx_A^+ \sin\left(\frac{L-x_A^+}{t_A}\right) \mathcal{S}^{(2)}(L, x_A^+; \mathbf{r}_q^A(\tau), \mathbf{r}_{\bar{q}}^A(\tau)) ,$$

where we identify the same functional form for the medium contribution as the one present in the direct term, see Eq. (3.15).

Out-out region: Setting the antenna to be outside the medium in both contributions leads to

$$2 \operatorname{Re} \sum \langle M_q M_{\bar{q}}^* \rangle_{\text{out-out}} = -2 C_F N_c \frac{(ge)^2}{z_q(1-z_q)E_\gamma^3} \frac{t_g \bar{t}_g t_A}{\bar{z}_g z_g} |J(p+\bar{p})|^2 \boldsymbol{\kappa} \cdot \bar{\boldsymbol{\kappa}} P_{\gamma \rightarrow q\bar{q}}(z_q) , \quad (3.24)$$

which coincides with the vacuum result for the interference term.

3.3 Medium Modifications to Squared Matrix Elements

The full result for the direct terms, including the emission off the quark line and that off the anti-quark, can be compactly written as

$$\langle |M_q|^2 \rangle + \langle |M_{\bar{q}}|^2 \rangle = 4 C_F g^2 \mathcal{M}_{q\bar{q}}^2 \left(\frac{1}{\boldsymbol{\kappa}^2} + \frac{1}{\bar{\boldsymbol{\kappa}}^2} \right) (1 + F_{\text{med}}) , \quad (3.25)$$

where we have introduced $\mathcal{M}_{q\bar{q}}^2$, which corresponds to the production of a $q\bar{q}$ antenna from a virtual photon in vacuum, and is given by

$$\mathcal{M}_{q\bar{q}}^2 = \frac{e^2 N_c t_A}{E_\gamma} P_{\gamma \rightarrow q\bar{q}}(z_q) |J(p+\bar{p})|^2 . \quad (3.26)$$

We have identified F_{med} , the known factor controlling the medium-induced modification to the $q\bar{q}$ antenna production [32]

$$F_{\text{med}} = 2 \int_0^L \frac{d\bar{x}_A^+}{t_A} \int_0^{\bar{x}_A^+} \frac{dx_A^+}{t_A} \cos\left(\frac{\Delta x_A^+}{t_A}\right) \mathcal{S}^{(2)}(\bar{x}_A^+, x_A^+; \mathbf{r}_q^A(\tau), \mathbf{r}_{\bar{q}}^A(\tau)) \quad (3.27)$$

$$\times \mathcal{Q}^{(4)}(L, \bar{x}_A^+; \mathbf{r}_q^A(\tau), \mathbf{r}_{\bar{q}}^A(\tau), \bar{\mathbf{r}}_q^A(\tau), \bar{\mathbf{r}}_{\bar{q}}^A(\tau))$$

$$- 2 \int_0^L \frac{dx_A^+}{t_A} \sin\left(\frac{L-x_A^+}{t_A}\right) \mathcal{S}^{(2)}(L, x_A^+; \mathbf{r}_q^A(\tau), \mathbf{r}_{\bar{q}}^A(\tau)) .$$

We will discuss the limiting behaviour of this expression in the following section.

By summing Eqs. (3.21), (3.23) and (3.24) we obtain the interference term, which reads

$$\langle 2 \operatorname{Re} M_q M_{\bar{q}}^* \rangle = -8 C_F g^2 \mathcal{M}_{q\bar{q}}^2 \frac{\boldsymbol{\kappa} \cdot \bar{\boldsymbol{\kappa}}}{\boldsymbol{\kappa}^2 \bar{\boldsymbol{\kappa}}^2} \left[1 + 2 \int_0^L \frac{d\bar{x}_A^+}{t_A} \int_0^{\bar{x}_A^+} \frac{dx_A^+}{t_A} \cos\left(\frac{\Delta x_A^+}{t_A}\right) \right. \quad (3.28)$$

$$\times \mathcal{S}^{(2)}(L, \bar{x}_A^+; \mathbf{r}_q^A(\tau), \mathbf{r}_{\bar{q}}^A(\tau)) \mathcal{S}^{(2)}(L, \bar{x}_A^+; \bar{\mathbf{r}}_q^A(\tau), \bar{\mathbf{r}}_{\bar{q}}^A(\tau)) \mathcal{S}^{(2)}(\bar{x}_A^+, x_A^+; \mathbf{r}_q^A(\tau), \mathbf{r}_{\bar{q}}^A(\tau))$$

$$\left. - 2 \int_0^L \frac{dx_A^+}{t_A} \sin\left(\frac{L-x_A^+}{t_A}\right) \mathcal{S}^{(2)}(L, x_A^+; \mathbf{r}_q^A(\tau), \mathbf{r}_{\bar{q}}^A(\tau)) \right] .$$

We then recast this expression as

$$\langle 2 \operatorname{Re} M_q M_{\bar{q}}^* \rangle = -8 C_F g^2 \mathcal{M}_{q\bar{q}}^2 \frac{\boldsymbol{\kappa} \cdot \bar{\boldsymbol{\kappa}}}{\boldsymbol{\kappa}^2 \bar{\boldsymbol{\kappa}}^2} (1 + F_{\text{med}}) \left(1 - \tilde{\Delta}_{\text{med}} \right) \quad (3.29)$$

where we have defined $\tilde{\Delta}_{\text{med}}$ as

$$\begin{aligned} \tilde{\Delta}_{\text{med}} &= \frac{2}{1 + F_{\text{med}}} \int_0^L \frac{d\bar{x}_A^+}{t_A} \int_0^{\bar{x}_A^+} \frac{dx_A^+}{t_A} \cos\left(\frac{\Delta x_A^+}{t_A}\right) \mathcal{S}^{(2)}(\bar{x}_A^+, x_A^+; \mathbf{r}_q^A(\tau), \mathbf{r}_{\bar{q}}^A(\tau)) \\ &\times \left[\mathcal{Q}^{(4)}(L, \bar{x}_A^+; \mathbf{r}_q^A(\tau), \mathbf{r}_{\bar{q}}^A(\tau), \bar{\mathbf{r}}_q^A(\tau), \bar{\mathbf{r}}_{\bar{q}}^A(\tau)) \right. \\ &\quad \left. - \mathcal{S}^{(2)}(L, \bar{x}_A^+; \mathbf{r}_q^A(\tau), \mathbf{r}_{\bar{q}}^A(\tau)) \mathcal{S}^{(2)}(L, \bar{x}_A^+; \bar{\mathbf{r}}_q^A(\tau), \bar{\mathbf{r}}_{\bar{q}}^A(\tau)) \right]. \end{aligned} \quad (3.30)$$

In the rest of this paper we will refer to $\tilde{\Delta}_{\text{med}}$ as the *generalized decoherence factor*. Indeed, as we will see in the next section, in the limit of $\Delta x_A^+ = \bar{x}_A^+ - x_A^+ \rightarrow 0$ it reduces to the Δ_{med} computed in Refs. [23–31].

We can interpret this formula as follows. First, the propagation of the virtual antenna during Δx_A^+ is described by a dipole correlator of Wilson lines. From \bar{x}_A^+ to L , the antenna is now real and there are two possible ways of connecting the colour of the four Wilson lines [51]. One, described by the quadrupole, in which the q in the amplitude is colour connected to the \bar{q} in the amplitude and similarly for the \bar{q} . The second colour configuration, described by the double-dipole, consists in considering the four-particle system as two separate $q\bar{q}$ dipoles, one in the amplitude and the other in the conjugated amplitude.

Putting direct contributions and interference terms together, we obtain our final result for the squared matrix element for the emission of a soft gluon off a (colour singlet) $q\bar{q}$ antenna,

$$\mathcal{M}_{q\bar{q}}^2 = 4 C_F g^2 \mathcal{M}_{q\bar{q}}^2 (1 + F_{\text{med}}) \left[\left(\frac{1}{\boldsymbol{\kappa}^2} + \frac{1}{\bar{\boldsymbol{\kappa}}^2} - 2 \frac{\boldsymbol{\kappa} \cdot \bar{\boldsymbol{\kappa}}}{\boldsymbol{\kappa}^2 \bar{\boldsymbol{\kappa}}^2} \right) + 2 \frac{\boldsymbol{\kappa} \cdot \bar{\boldsymbol{\kappa}}}{\boldsymbol{\kappa}^2 \bar{\boldsymbol{\kappa}}^2} \tilde{\Delta}_{\text{med}} \right]. \quad (3.31)$$

This is the main result of this paper. It contains two pieces: (i) the full vacuum spectrum multiplied by the nuclear modification factor $(1 + F_{\text{med}})$, and (ii) a pure interference contribution multiplied by the generalized decoherence factor, which depends on the medium properties and the kinematics of the antenna.

3.4 Limiting behaviour

We now discuss how to recover two important limits of Eq. (3.31), namely the vacuum baseline and the limit where we set Δx_A^+ to zero.

In the vacuum limit, all dipoles and quadrupoles in Eqs. (3.27) and (3.30) become unity, and it follows that F_{med} and $\tilde{\Delta}_{\text{med}}$ vanish. Eq. (3.31) then reproduces the well known squared matrix element for soft gluon radiation off a colour singlet dipole in vacuum, see e.g. Refs. [21, 22].

Let us now turn to the limit where $\Delta x_A^+ = 0$. This is the setup considered in Refs. [23–31], where the antenna forms at $x_A^+ = 0$ (and hence $\bar{x}_A^+ = 0$) and the decoherence factor was found to be

$$\Delta_{\text{med}} = 1 - \mathcal{S}^{(2),\text{adj}}(L, 0; \mathbf{r}_q^A(\tau), \mathbf{r}_{\bar{q}}^A(\tau)). \quad (3.32)$$

Recovering this limiting behaviour from Eq. (3.31) requires some care, as some of the steps in our calculation are only valid if the antenna forms at different times in the amplitude and complex-conjugate amplitude. In particular, we note that out of the **in-in**, **in-out** and **out-out** regions only the **in-in** region survives. Furthermore, when computing the **in-in** contributions we fixed $\bar{x}_A^+ > x_A^+$ and accounted for the other ordering by multiplying the expressions by a factor of 2 (see e.g. Eqs. (3.6) and (3.19)). This factor must be removed if the time at which the antenna is formed is the same in the amplitude and complex-conjugate amplitude. Finally, to fix the time of formation we insert $t_A\delta(x_A^+)$ and $t_A\delta(\bar{x}_A^+)$ in our expressions for the **in-in** contributions. Following this procedure, we find that the direct contributions become

$$\langle |M_q|^2 \rangle + \langle |M_{\bar{q}}|^2 \rangle \rightarrow 4 C_F g^2 \mathcal{M}_{q\bar{q}}^2 \left(\frac{1}{\kappa^2} + \frac{1}{\bar{\kappa}^2} \right), \quad (3.33)$$

where we used that

$$\mathcal{S}^{(2)}(0, 0; \mathbf{r}_q^A(\tau), \mathbf{r}_{\bar{q}}^A(\tau)) = 1, \quad \mathcal{Q}^{(4)}(L, 0; \mathbf{r}_q^A(\tau), \mathbf{r}_{\bar{q}}^A(\tau), \mathbf{r}_q^A(\tau), \mathbf{r}_{\bar{q}}^A(\tau)) = 1. \quad (3.34)$$

As expected, we recover the fact that in this limit there are no medium modifications to the direct terms. Effectively, this amounts to taking $1 + F_{\text{med}} \rightarrow 1$. To compute the limit of the interference contribution, we set $1 + F_{\text{med}} \rightarrow 1$ and then apply the limiting procedure described above to the integrals in $\tilde{\Delta}_{\text{med}}$. Using Eq. (3.34) and noting that, in the large- N_c limit,

$$\left[\mathcal{S}^{(2)}(L, 0; \mathbf{r}_q^A(\tau), \mathbf{r}_{\bar{q}}^A(\tau)) \right]^2 = \mathcal{S}^{(2),\text{adj}}(L, 0; \mathbf{r}_q^A(\tau), \mathbf{r}_{\bar{q}}^A(\tau)), \quad (3.35)$$

we find that

$$\tilde{\Delta}_{\text{med}} \rightarrow \Delta_{\text{med}}, \quad (3.36)$$

with Δ_{med} as defined in Eq. (3.32). We finally get

$$\langle 2 \text{Re} M_q M_{\bar{q}}^* \rangle \rightarrow -8 C_F g^2 \mathcal{M}_{q\bar{q}}^2 \frac{\kappa \cdot \bar{\kappa}}{\kappa^2 \bar{\kappa}^2} (1 - \Delta_{\text{med}}), \quad (3.37)$$

in full agreement with the results of Refs. [23–31].

4 Medium model and numerical results

4.1 Medium model

To numerically evaluate the expressions presented in the previous section, we need to specify a medium model. Following standard practice in the jet-quenching literature, we opt for taking the harmonic oscillator approximation for the in-medium potential. We further consider a static medium, i.e., a medium with constant transport properties along different trajectories, modeled by the parameter \hat{q} . Note that the transport coefficient depends on the colour representation, and we choose \hat{q} to be that corresponding to the fundamental degrees of freedom. The adjoint case is simply given by $C_A \hat{q} / C_F$, which in the large- N_c limit reduces to $2\hat{q}$. Furthermore, it is convenient to work in the frame where the virtual photon has zero transverse momentum (see e.g. the discussion in Ref. [32]).

Under the harmonic approximation, the dipole correlator of two Wilson lines becomes [51–53]

$$\mathcal{S}^{(2)}(t, t_1; \mathbf{r}_1, \mathbf{r}_2) = e^{-\frac{1}{4}\hat{q} \int_{t_1}^t d\tau [\mathbf{r}_1(\tau) - \mathbf{r}_2(\tau)]^2}, \quad (4.1)$$

where $\mathbf{r}_{1,2}$ correspond to Wilson-line trajectories (either in the amplitude or the conjugate amplitude) as defined in Eqs. (2.12) and (3.7). In the large- N_c limit, the quadrupole can be written in terms of these dipoles as [51–53]

$$\begin{aligned} \mathcal{Q}^{(4)}(L, \bar{x}_A^+; \mathbf{r}_q^A(\tau), \bar{\mathbf{r}}_q^A(\tau), \bar{\mathbf{r}}_q^A(\tau), \bar{\mathbf{r}}_q^A(\tau)) &= \mathcal{S}^{(2)}(L, \bar{x}_A^+; \mathbf{r}_q^A, \bar{\mathbf{r}}_q^A) \mathcal{S}^{(2)}(L, \bar{x}_A^+; \mathbf{r}_q^A, \bar{\mathbf{r}}_q^A) \\ &+ \int_{\bar{x}_A^+}^L ds \mathcal{S}^{(2)}(L, s; \mathbf{r}_q^A, \bar{\mathbf{r}}_q^A) \mathcal{S}^{(2)}(L, s; \mathbf{r}_q^A, \bar{\mathbf{r}}_q^A) T(s) \mathcal{S}^{(2)}(s, \bar{x}_A^+; \mathbf{r}_q^A, \bar{\mathbf{r}}_q^A) \mathcal{S}^{(2)}(s, \bar{x}_A^+; \bar{\mathbf{r}}_q^A, \bar{\mathbf{r}}_q^A), \end{aligned} \quad (4.2)$$

where

$$T(s) = -\frac{\hat{q}}{2} \left[(\mathbf{r}_q^A - \bar{\mathbf{r}}_q^A)^2 + (\bar{\mathbf{r}}_q^A - \bar{\mathbf{r}}_q^A)^2 - (\mathbf{r}_q^A - \bar{\mathbf{r}}_q^A)^2 - (\bar{\mathbf{r}}_q^A - \mathbf{r}_q^A)^2 \right], \quad (4.3)$$

is the well-known transition amplitude.

These expressions can be made more explicit by inserting the trajectories for the Wilson lines. As an example, for the dipole $\mathcal{S}^{(2)}(L, x_A^+; \mathbf{r}_q^A, \bar{\mathbf{r}}_q^A)$, the difference of transverse coordinates that appears is given by

$$(\mathbf{r}_q^A - \bar{\mathbf{r}}_q^A)^2 = (\tau - x_A^+)^2 \theta_{q\bar{q}}^2, \quad (4.4)$$

and therefore the dipole becomes

$$\mathcal{S}^{(2)}(L, x_A^+; \mathbf{r}_q^A, \bar{\mathbf{r}}_q^A) = e^{-\frac{1}{12}\hat{q}\theta_{q\bar{q}}^2(L-x_A^+)^3}. \quad (4.5)$$

Another correlator of Wilson lines that enters Eq. (3.30) is the double-dipole, which under the aforementioned limits and approximations reads [50]

$$\mathcal{S}^{(2)}(L, \bar{x}_A^+; \mathbf{r}_q^A, \bar{\mathbf{r}}_q^A) \mathcal{S}^{(2)}(L, \bar{x}_A^+; \bar{\mathbf{r}}_q^A, \bar{\mathbf{r}}_q^A) = e^{-\frac{1}{12}\hat{q}\theta_{q\bar{q}}^2[(L-\bar{x}_A^+)^3 - (\bar{x}_A^+ - x_A^+)^3 + (L-x_A^+)^3]}. \quad (4.6)$$

Finally, starting from Eq. (4.2), the quadrupole entering Eqs. (3.27) and (3.30) is [51–53]

$$\begin{aligned} \mathcal{Q}^{(4)}(L, \bar{x}_A^+; \mathbf{r}_q^A, \bar{\mathbf{r}}_q^A, \bar{\mathbf{r}}_q^A, \bar{\mathbf{r}}_q^A) &= e^{-\frac{1}{4}\hat{q}\theta_{q\bar{q}}^2[z_q^2 + (1-z_q)^2](\bar{x}_A^+ - x_A^+)^2(L-\bar{x}_A^+)} \\ &+ T(\bar{x}_A^+, x_A^+) \int_{\bar{x}_A^+}^L ds e^{-\frac{1}{4}\hat{q}\theta_{q\bar{q}}^2[z_q^2 + (1-z_q)^2](L-s)(\bar{x}_A^+ - x_A^+)^2} e^{-\frac{1}{12}\hat{q}\theta_{q\bar{q}}^2[(s-\bar{x}_A^+)^3 + (s-x_A^+)^3 - (L-s)^3]}, \end{aligned} \quad (4.7)$$

with the transition amplitude becoming

$$T(\bar{x}_A^+, x_A^+) = -\hat{q}z_q(1-z_q)\theta_{q\bar{q}}^2(\bar{x}_A^+ - x_A^+)^2. \quad (4.8)$$

In the previous equations we have introduced the opening angle of the antenna, $\theta_{q\bar{q}} = |\boldsymbol{\theta}_{q\bar{q}}|$, that is defined as the modulus of

$$\boldsymbol{\theta}_{q\bar{q}} \equiv \frac{\mathbf{p}}{z_q E_\gamma} - \frac{\bar{\mathbf{p}}}{(1-z_q)E_\gamma}. \quad (4.9)$$

We note that everything in the latter expression is defined in light-cone coordinates. The light-cone energies and angles are related to the usual energy p^0 and Cartesian angle $\theta_{q\bar{q}}^{\text{cart}}$

by a rescaling (see footnote 3), $E = p^+ \sim \sqrt{2}p^0$ and $\theta_{q\bar{q}} = \theta_{q\bar{q}}^{\text{cart}}/\sqrt{2}$. Following this convention, the antenna formation time t_A defined in Eq. (2.14) becomes

$$t_A = \frac{2}{z_q(1-z_q)\theta_{q\bar{q}}^2 E_\gamma}. \quad (4.10)$$

Within the specific medium model we have chosen, the various correlators of Wilson lines discussed above are governed by characteristic physical scales. As an example, we note that Δ_{med} can be written as

$$\Delta_{\text{med}} = 1 - e^{-\frac{1}{6}\hat{q}\theta_{q\bar{q}}^2 L^3} = 1 - e^{-\theta_{q\bar{q}}^2/\theta_c^2}, \quad (4.11)$$

where we have introduced the well-known critical angle [54]

$$\theta_c = \sqrt{\frac{6}{\hat{q}L^3}}. \quad (4.12)$$

Other relevant scales can be identified in both F_{med} and $\tilde{\Delta}_{\text{med}}$. These have already been investigated in detail in Refs. [32, 33] within the context of the calculation of F_{med} so we do not discuss them again here.

4.2 Numerical results and discussion

In this section we present a numerical study of our main result, $\tilde{\Delta}_{\text{med}}(E_\gamma, z_q, \theta_{q\bar{q}})$, as defined in Eq. (3.30), within the medium model discussed above. Together with this manuscript, we include an ancillary file, `tildeDeltaMedNum.m`, that contains a simple numerical implementation of $\tilde{\Delta}_{\text{med}}$ (and F_{med} , see Eq. (3.27)) in `Mathematica` that should allow the reader to reproduce our results in the bulk of the parameter space we explore. The numerical results discussed below were obtained with a more robust numerical implementation.

We first evaluate the generalized decoherence factor $\tilde{\Delta}_{\text{med}}(E_\gamma, z_q, \theta_{q\bar{q}})$ and compare it to the standard $\Delta_{\text{med}}(\theta_{q\bar{q}})$ for a medium with fixed $\hat{q} = 1.5 \text{ GeV}^2/\text{fm}$, varying lengths $L = (2, 4, 6) \text{ fm}$ and with photon energies $E_\gamma = (200, 400, 800) \text{ GeV}$.⁴ These medium parameters were chosen to be consistent with other jet-quenching phenomenological studies using the static brick approximation, see e.g. Refs. [55–58]. Our results are presented in Fig. 4.

Before delving into the behavior of $\tilde{\Delta}_{\text{med}}$, let us briefly comment on the standard Δ_{med} result. This function only depends on the medium properties, and, as such, it remains invariant when increasing E_γ (moving from left to right in Fig. 4). Its parametric dependence on the medium is also transparent: given that \hat{q} is fixed, the larger the L , the smaller the value of θ_c (see Eq. (4.12)). In other words, for larger L we get full decoherence of the gluon radiation at smaller antenna opening angles.

We start the description of $\tilde{\Delta}_{\text{med}}$ by focusing on the collinear regime ($\theta_{q\bar{q}} \ll 1$). We observe that $\tilde{\Delta}_{\text{med}}$ is systematically bigger than Δ_{med} for all values of z_q . This observation

⁴Note that we take these values for the light-cone coordinates used throughout this paper, see the comment below Eq. (4.9).

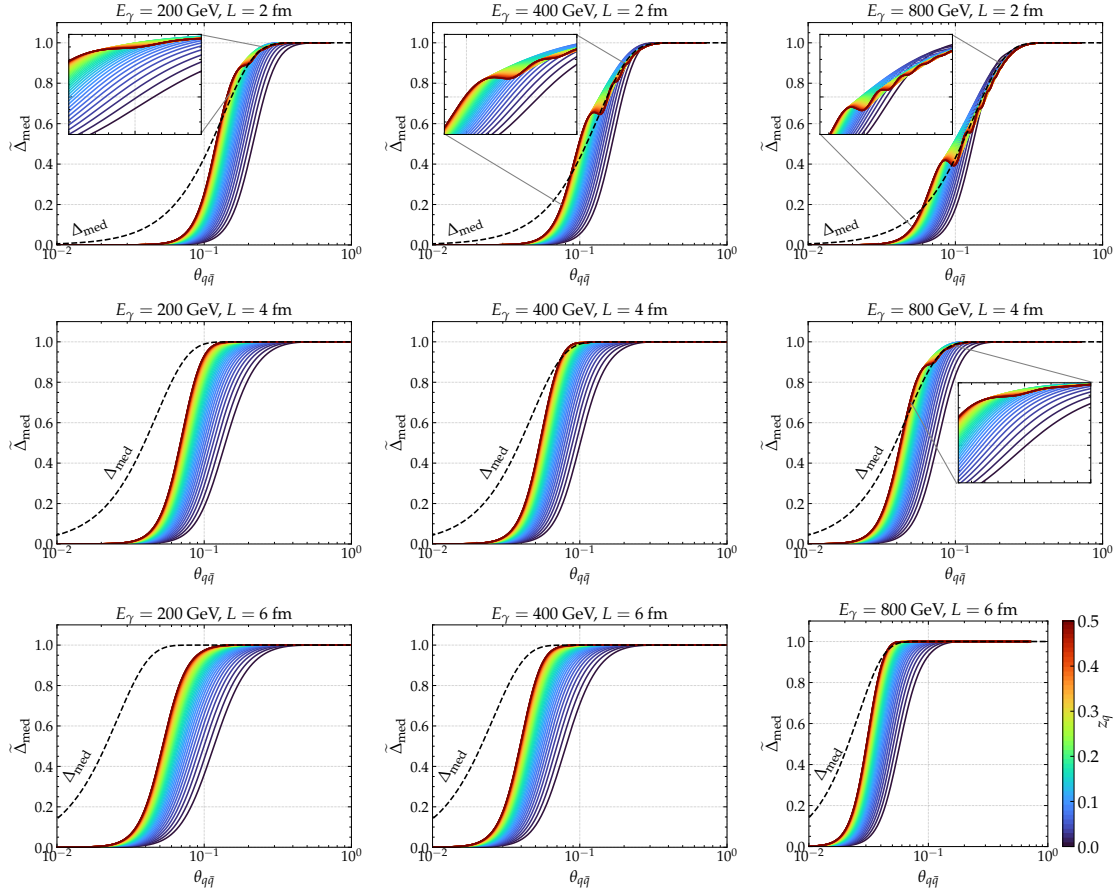


Figure 4: Numerical evaluation of the generalized decoherence factor $\tilde{\Delta}_{\text{med}}$ in Eq. (3.30) as a function of the opening angle of the antenna, $\theta_{q\bar{q}}$, and its energy sharing fraction, z_q , for three different photon energies and medium lengths. The dashed black line corresponds to Δ_{med} , see Eq. (3.32). The value of \hat{q} is fixed to $1.5 \text{ GeV}^2/\text{fm}$.

can be understood analytically by expanding Eqs. (3.31) and (3.32) in the small-angle limit. We find that they behave as

$$\begin{aligned}
 \tilde{\Delta}_{\text{med}} \Big|_{\theta_{q\bar{q}} \ll 1} &= \frac{1}{480} \hat{q} L^5 E_\gamma^2 z_q^2 (1 - z_q)^2 (3 - 2z_q + 2z_q^2) \theta_{q\bar{q}}^6 + \mathcal{O}(\theta_{q\bar{q}}^8) \\
 \Delta_{\text{med}} \Big|_{\theta_{q\bar{q}} \ll 1} &= \frac{1}{6} \hat{q} L^3 \theta_{q\bar{q}}^2 + \mathcal{O}(\theta_{q\bar{q}}^4)
 \end{aligned}
 \tag{4.13}$$

We note that the radius of convergence of these expansions is very small: while for $\theta_{q\bar{q}} < 0.01$ they give a good approximation of the exact result, for $\theta_{q\bar{q}} > 0.01$ the series stops converging very quickly for realistic values of E_γ and \hat{q} . Nevertheless, the small-angle expansions provide an explanation for the behaviour we observe in all the plots of Fig. 4, i.e., $\tilde{\Delta}_{\text{med}} < \Delta_{\text{med}}$ in the $\theta_{q\bar{q}} \rightarrow 0$ limit. Physically, this implies that gluons radiated off very hard-collinear prongs of a $q\bar{q}$ -antenna are vacuum-like (since F_{med} also vanishes in this limit, as shown in Fig. 7).

In the opposite regime, $\theta_{q\bar{q}} \rightarrow 1$, both decoherence factors $\tilde{\Delta}_{\text{med}}$ and Δ_{med} reach unity. Consequently, the medium-induced correction to the antenna emission pattern exactly cancels the vacuum interference term, and thus the radiation pattern of the antenna becomes that of two independent colour charges. For the parameter space we explore, this regime is reached for small values of $\theta_{q\bar{q}}$, well before $\theta_{q\bar{q}} = 1$, where the small angle approximation we have taken in our calculation is still valid. We then conclude that the regime of total colour decoherence ($\tilde{\Delta}_{\text{med}} = 1$) is reached even when incorporating medium modifications during the formation of the antenna. However, the value of $\theta_{q\bar{q}}$ for which $\tilde{\Delta}_{\text{med}} \rightarrow 1$ is now a function not only of the medium properties but also of z_q and E_γ .

Understanding the large-angle ($\theta_{q\bar{q}} \rightarrow 1$) behaviour of both F_{med} and $\tilde{\Delta}_{\text{med}}$ analytically is not trivial given the integrals appearing in their definition. Instead, we have numerically explored this limit, observing that $F_{\text{med}} \rightarrow 0$ for sufficiently large values of z_q (see Fig. 7 and the discussion in Appendix A). We have also probed the large-angle limit of each of the two contributions appearing in the numerator of $\tilde{\Delta}_{\text{med}}$ numerically. We found that terms proportional to the quadrupole go to 1, while those proportional to the double dipole go to 1/2, reproducing the expected behaviour, $\tilde{\Delta}_{\text{med}} \rightarrow 1$.

Perhaps one of the most interesting and novel features of Fig. 4 is the transition region at intermediate angles, where the colour decoherence factor is neither 0 nor 1. For the values of the parameters explored in this work, we identify two regimes that we proceed to discuss separately. First, for dense enough media ($\hat{q}L = 6, 9 \text{ GeV}^2$, with $\hat{q} = 1.5 \text{ GeV}^2/\text{fm}$) and photon energies of $E_\gamma = 200, 400 \text{ GeV}$ we find that $\tilde{\Delta}_{\text{med}}$ monotonically grows with z_q . In other words, for fixed $\theta_{q\bar{q}}$, radiation with larger values of z_q will have a larger proportion of anti-angular ordered emissions.⁵ In addition, even at $z_q = 0.5$, there is a gap between the Δ_{med} and $\tilde{\Delta}_{\text{med}}$ curves, whose size varies with both L and E_γ . This gap, more pronounced for $L = 6 \text{ fm}$ and $E_\gamma = 200, 400 \text{ GeV}$, leads to a clear delay of the onset of total decoherence. Finally, we observe that in this regime Δ_{med} and $\tilde{\Delta}_{\text{med}}$ are not just shifted but also have different slopes. When fixing \hat{q} and L so as to fix Δ_{med} , we find that $\tilde{\Delta}_{\text{med}}$ gets closer to Δ_{med} when increasing E_γ . We interpret this observation as a consequence of the reduction of the antenna formation time with increasing E_γ , since then the impact of considering $\Delta x_A^+ \neq 0$ is suppressed, i.e., the antenna formation is less sensitive to medium effects and $\tilde{\Delta}_{\text{med}} \rightarrow \Delta_{\text{med}}$.

When reducing the medium length to $L = 2 \text{ fm}$ (and also for $L = 4 \text{ fm}$, $E_\gamma = 800 \text{ GeV}$), we observe new interesting features. First, a non-monotonic dependence of $\tilde{\Delta}_{\text{med}}$ on z_q . As clearly shown in the inset plots, curves for moderate values of z_q can surpass that corresponding to the democratic branching case at relatively small angles, $\theta_{q\bar{q}} \sim 0.1$. The insets also showcase an oscillatory behaviour of $\tilde{\Delta}_{\text{med}}$ that becomes more pronounced when increasing the photon energy. We would like to highlight that these oscillations are already present in F_{med} when evaluated in this kinematic regime (see Fig. 7). Indeed, they result from the interplay between the frequency of the trigonometric functions (which is independent of the medium parameters \hat{q} and L , but depends on E_γ and $\theta_{q\bar{q}}$ through t_A),

⁵An important remark is that very asymmetric splittings, when $z_q \sim 0$ (or $z_q \sim 1$), are beyond the regime of validity of our calculation since, in these cases, one of the two prongs is very soft and thus the tilted Wilson line approximation for the propagators is not justified.

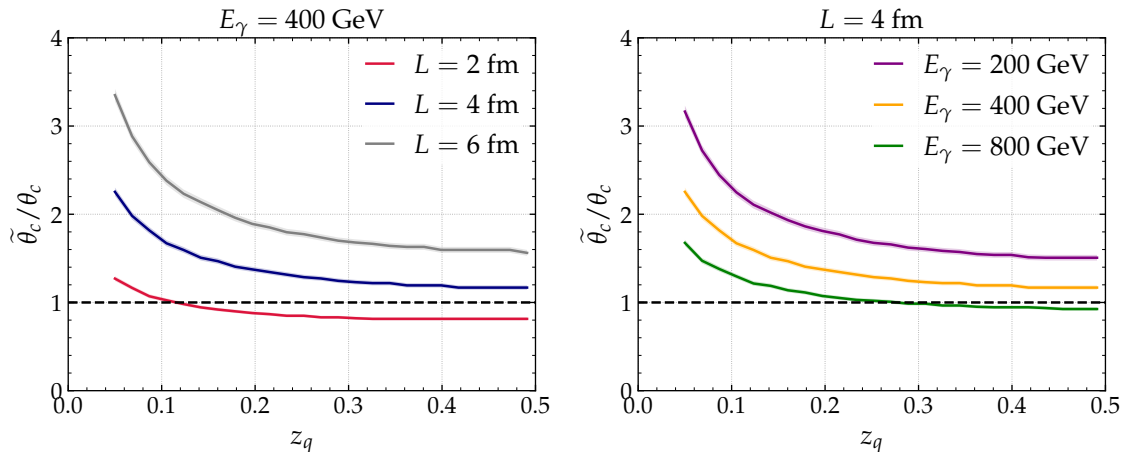


Figure 5: Ratio between the generalized critical angle and the standard one (see Eq. (4.12)) as a function of the energy sharing fraction for different medium lengths and photon energies.

and the exponential decay of the Wilson-line correlators (that depend solely on the medium parameters).⁶ Quantitatively, the most important observation is that the gap between Δ_{med} and $\tilde{\Delta}_{\text{med}}$ significantly shrinks, especially for the highest value of E_γ . In other words, Δ_{med} becomes a good approximation for $\tilde{\Delta}_{\text{med}}$ despite its non-trivial parametric dependences.

A way of further characterizing the colour decoherence factor is by identifying a generalisation of the critical angle defined in Eq. (4.12). In analogy with θ_c , we define $\tilde{\theta}_c$ as the angle for which $\tilde{\Delta}_{\text{med}}(E_\gamma, z_q, \theta_{q\bar{q}} = \tilde{\theta}_c) = 1 - e^{-1}$. Traditionally, this angle has been interpreted as a property of the medium that controls its resolution power: splittings with $\theta_{q\bar{q}} < \theta_c$ were said not to be resolved by the medium. After accounting for finite formation time effects, this picture becomes more complex since this angle is not only a property of the medium but also depends on E_γ and z_q , and thus changes on a splitting-by-splitting basis.

The extracted values of $\tilde{\theta}_c/\theta_c$ are presented in Fig. 5. This ratio allows us to quantify the aforementioned gap between Δ_{med} and $\tilde{\Delta}_{\text{med}}$. In the left panel, the energy of the photon is fixed and the medium properties vary. In this way, both θ_c and $\tilde{\theta}_c$ change. The ratio between these two quantities shows an enhancement due to finite formation time effects for small values of z_q , and then a flattening as $z_q \rightarrow 0.5$. However, since our results are not valid for $z_q \rightarrow 0$, we should treat the small z_q behaviour with care. The difference between θ_c and $\tilde{\theta}_c$ can be substantial. For instance, focusing on $z_q \geq 0.2$, and on long media ($L = 6$ fm), we find that the new critical angle is larger by a factor of order 2. The case $L = 2$ fm

⁶ We have performed numerical checks to verify that the oscillations are not due to numerical instabilities. More precisely, we have used various numerical integration strategies (as implemented in `Mathematica`) and checked that they give the same results, and we have studied the error associated with the numerical integration to be sure that it is well below the amplitude of the observed oscillations. Furthermore, we note that the oscillations appear in regions of small $\theta_{q\bar{q}}$ where the numerical integrations converge well. For some choices of medium parameters, as $\theta_{q\bar{q}} \rightarrow 1$ the convergence becomes problematic and we have excluded those points since then we always have that $\tilde{\Delta}_{\text{med}} \rightarrow 1$.

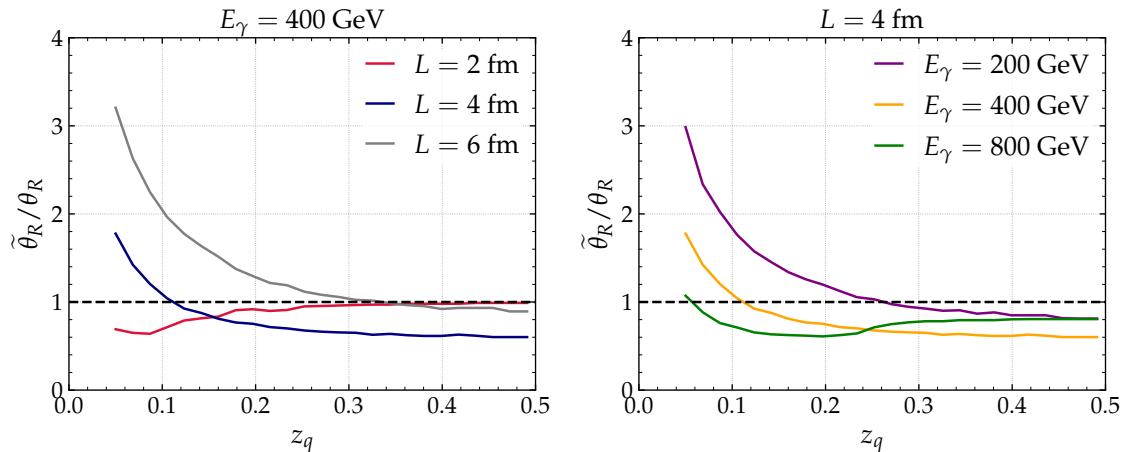


Figure 6: Ratio between the rise angle extracted for $\tilde{\Delta}_{\text{med}}$ and Δ_{med} as a function of the energy sharing fraction for different medium lengths and photon energies.

is again qualitatively different from the other two since $\tilde{\theta}_c/\theta_c$ becomes slightly smaller than one. It is important to note that, for this medium setup, the $\tilde{\Delta}_{\text{med}}$ curves oscillate with a non-negligible amplitude, and thus the meaning of $\tilde{\theta}_c$ becomes less transparent. Indeed, given the oscillatory nature of the curves, we can encounter situations where $\tilde{\Delta}_{\text{med}} = 1 - e^{-1}$ for two different angles. The right panel of Fig. 5 shows the dependence of $\tilde{\theta}_c/\theta_c$ on the energy of the photon for fixed values of \hat{q} and L . In this case, the denominator of this ratio is fixed and only the numerator varies. We observe that the ratio becomes smaller with increasing E_γ . This is again compatible with the gap between $\tilde{\Delta}_{\text{med}}$ and Δ_{med} becoming narrower for shorter formation times of the antenna.

The characterization of the differences between $\tilde{\Delta}_{\text{med}}$ and Δ_{med} in terms of a single critical angle is somehow incomplete. Indeed, as we have mentioned earlier, $\tilde{\Delta}_{\text{med}}$ and Δ_{med} are not related by a simple shift (see Fig. 4). Furthermore, given the more involved dependence of $\tilde{\Delta}_{\text{med}}$ on $\theta_{q\bar{q}}$, a smaller value of $\tilde{\theta}_c$ does not imply that $\tilde{\Delta}_{\text{med}}$ reaches the regime of total colour decoherence faster. For these reasons, we introduce another variable that we call ‘the rise angle’, θ_R . This variable measures the angular interval in which the colour decoherence factor rises from a given value $\Delta_{\text{med}}^{\text{min}}$ to $\Delta_{\text{med}}^{\text{max}}$ (and similarly for $\tilde{\Delta}_{\text{med}}$), informing us about the slope of the distribution: the smaller θ_R is, the faster the distribution rises. We perform our extraction of θ_R in the $\Delta_{\text{med}}^{\text{min}} = 0.2$ and $\Delta_{\text{med}}^{\text{max}} = 0.95$ window so as to capture the transition region. As we did for θ_c , we present the ratio between the value for the rise angle using $\tilde{\Delta}_{\text{med}}$, denoted $\tilde{\theta}_R$, and the one obtained from Δ_{med} , denoted θ_R .

The results are displayed in Fig. 6 in the same format as for Fig. 5: in the left panel we fix the photon energy and change the medium parameters, and in the right panel we do the opposite. Let us again focus on the region of semi-hard splittings. The first thing to notice on the left panel is that the curve for $L = 2$ fm is compatible with one. This supports the idea that Δ_{med} is a good approximation of $\tilde{\Delta}_{\text{med}}$ for this regime. For $L = 4$ fm, we find that $\tilde{\Delta}_{\text{med}}$ rises almost twice as fast as Δ_{med} ($\tilde{\theta}_R/\theta_R \sim 0.5$), and $\tilde{\Delta}_{\text{med}}$ is closer

to a Heaviside function in this particular scenario. The picture is reversed when further increasing the value of L , i.e., $\tilde{\theta}_R/\theta_R$ is bigger or equal to 1 for $L = 6$ fm. We see that the rise angle provides complementary information compared to that extracted from the critical angle. While from the critical angle perspective it seems that, for $L = 4$ fm, $\tilde{\Delta}_{\text{med}}$ behaves similarly to Δ_{med} , we observe that the rise angle manifests the much sharper rise of $\tilde{\Delta}_{\text{med}}$. Conversely, the rise angle does not allow to capture the gap between $\tilde{\Delta}_{\text{med}}$ and Δ_{med} that is clearly present for $L = 6$ fm, but this is neatly exposed by the critical angle.

The right panel of Fig. 6 keeps θ_R fixed. Interestingly, we observe that $\tilde{\theta}_R/\theta_R < 1$ for sufficiently large z_q values, that is $\tilde{\Delta}_{\text{med}}$ rises faster than Δ_{med} . This information could not have been extracted from the θ_c analysis, since from that we could only tell that the critical angle was larger. Putting together both observations, we conclude that even if $\tilde{\theta}_c > \theta_c$, the generalized decoherence factor grows faster towards the total decoherence regime.

5 Conclusions

One of the most striking modifications induced by the QGP on a QCD parton shower is the breaking of angular-ordering. This was observed in a series of pioneering papers almost 15 years ago by studying the radiation pattern off a QCD antenna in the presence of a medium [23–31]. The parameter that emerged from these studies was the so-called critical angle θ_c , a property of the medium that dictates whether it is able to resolve a certain splitting or not. In this way, splittings with $\theta < \theta_c$ are not resolved and mostly respect angular ordering for subsequent emissions. Conversely, splittings with $\theta > \theta_c$ are resolved, and the radiation pattern of the antenna becomes that of two independent colour charges. The physical picture is that, for resolved splittings, interactions with the medium induce rotations of the colour state of each prong of the antenna, and they effectively become decorrelated sources in colour space. Constraining the values of θ_c , and more generally the physics of colour decoherence, is one of the targets of the heavy-ion experimental program at the LHC [59–62].

In this work, we have revisited the calculation of Refs. [23–31], but accounted for medium effects during the formation of the antenna. While we have restricted our calculation to a colour singlet antenna radiating a soft gluon outside of the medium, we already observed some new striking effects. In particular, we have shown that the notion of a critical angle that exclusively depends on the medium properties no longer holds after considering that the antenna itself can interact with the medium while being formed. We have introduced a generalized decoherence factor, $\tilde{\Delta}_{\text{med}}$, that depends on both the medium properties (\hat{q}, L) and the kinematics of the antenna ($E_\gamma, z_q, \theta_{q\bar{q}}$). Consequently, each splitting in the parton shower experiences colour decoherence in a different fashion. More concretely, when considering a dense medium ($\hat{q} = 1.5$ GeV²/fm, $L = 6$ fm) we find that $\tilde{\Delta}_{\text{med}}$ remains zero for a broader interval of $\theta_{q\bar{q}}$ values than Δ_{med} . The direct implication is that these very collinear splittings do not violate angular ordering, i.e., their radiation behaves like vacuum emissions. In addition, we observe that there are at least two ways to reduce the differences between $\tilde{\Delta}_{\text{med}}$ and Δ_{med} : increasing the energy of the photon or reducing L . The interpretation of the former is very clear, as it is equivalent to reducing the antenna

formation time and thus it is natural that medium modifications effects to the antenna formation are less pronounced.

Given the fact that $\tilde{\Delta}_{\text{med}}$ and Δ_{med} are not simply related by a shift, even at fixed z_q , characterizing their differences in terms of differences of critical angles is insufficient. We have introduced a new metric, the rise angle θ_R , that measures how fast the decoherence factor grows between two set values (we take them to be 0.2 and 0.95). The rise angle becomes smaller the faster the function grows, becoming zero for a Heaviside function. Within the explored region of phase-space, we find a non-trivial parametric dependence of $\tilde{\theta}_R$, the rise angle associated with $\tilde{\Delta}_{\text{med}}$. More precisely, we find that it can be larger or smaller than the equivalent interval for Δ_{med} depending on the medium and antenna properties. This indicates that accounting for medium modifications during the antenna formation can either delay or accelerate colour decoherence.

Besides the interference effects, we find that the total rate of emissions off the antenna is enhanced by a factor F_{med} , that was first introduced in Refs [32, 33]. This function also has a non-trivial parametric dependence and can be as large as a factor of $\mathcal{O}(10)$ for non-extreme values of the parameter space, e.g. $E_\gamma = 200$ GeV, $L = 6$ fm, $z_q = 0.2$ and $\theta_{q\bar{q}} = 0.15$. Thus, medium modifications not only alter the balance between angular ordered and anti-angular ordered emissions but also induce more radiation overall.

This generalized picture of colour decoherence has multiple consequences. As an important example, this class of interference effects is crucial when formulating an in-medium parton shower. Several implementations of colour decoherence exist in the literature [34, 63, 64]. The one closest in spirit to the dynamics encapsulated in Δ_{med} is that of the JetMed parton shower where the first vacuum-like emission outside of the medium can happen at any angle while angular ordering is preserved for all subsequent emissions [34]. In light of the new functional dependence of $\tilde{\Delta}_{\text{med}}$, the idea of always breaking angular ordering for the first emission outside of the medium should be revisited. Phenomenologically, colour decoherence affects observables such as the fragmentation function [65] and, more generally, the jet substructure [56, 57, 66–71]. All these calculations use θ_c as an angular cutoff to determine whether the two prongs in a splitting lose energy by emitting medium-induced emissions. Once again, the fact that $\tilde{\theta}_c$ has a more intricate parametric dependence will impact these results. Furthermore, one should also study the impact of the increase in the rate of gluon emissions related to F_{med} in in-medium parton showers.

In order to make the generalized picture of colour decoherence applicable to realistic LHC scenarios there are a few aspects of the calculation that should be improved. First, we need to extend the calculation to other splitting channels relevant for jet production. Second, it would also be interesting to explore the case in which the emission takes place inside the medium. Steps in this direction have been taken in Ref. [72]. In that work, the authors studied coherence effects for $q \rightarrow qg_1g_2$ splittings with the gluon g_1 emitted inside the medium and the gluon g_2 outside. The more complex colour algebra of this splitting channel hampered the possibility of identifying in a clean fashion the corresponding F_{med} and $\tilde{\Delta}_{\text{med}}$ factors, as we were able to do in Eq. (3.31) for a colour singlet antenna. An approximation that could help to simplify the calculation would be to consider that the two splittings have short formation times. Aside from the generalization to other splittings, it

would also be interesting to explore the consequences of relaxing the eikonal approximation for the prongs of the antenna and the soft limit for the emitted gluon, so that we have a better control of these effects in all regions of phase space.

Another extension of this work concerns heavy quarks. In this case, colour decoherence competes with dead-cone effects that manifest as a suppression of radiation below the dead-cone angle, $\theta_0 \sim m_Q/E_Q$. Calculating the corresponding $\tilde{\Delta}_{\text{med}}$ for a heavy-quark antenna would then impact recent phenomenological proposals to measure the filling of the dead-cone in heavy-ion collisions [73, 74]. This is so because the possibility of filling the dead-cone with medium-induced emissions requires that those emissions have angles satisfying $\theta_c < \theta < \theta_0$ region [75]. In the standard picture, this hierarchy can be achieved by exploiting the fact that the critical angle θ_c only depends on the properties of the medium, while the dead-cone angle depends on the energy and the mass of the emitter. Given that $\tilde{\theta}_c$ now also depends on the kinematics of the emitter, the fine-tuning of angular scales becomes more delicate.

Yet another direction would be to relate our work to the different perspective on the ‘antenna laboratory’ that has been recently presented in Ref. [76]. This work studies the impact of colour coherence effects on the recoiling parton from the QGP, thus shifting the focus from the high-energy probe. We plan to carry out a dedicated study on how to incorporate these coherence effects in our setup.

Finally, we note that there have been several efforts in the past to understand the angular structure of the in-medium QCD cascade beyond the antenna setups discussed above. For example, the $1 \rightarrow 3$ in-medium splitting functions in the collinear limit were computed in Ref. [77] at first order in opacity. In this limit, vacuum/medium radiation is neither angular nor anti-angular ordered. This calculation was also revisited in Ref. [78] imposing additional constraints on the energy ordering of the outgoing particles. The very challenging task of computing the matrix element for two medium-induced emissions with generic kinematics is an on-going effort [79–81]. It would be interesting to understand in which limit the expressions presented in those works reduce to $\tilde{\Delta}_{\text{med}}$.

In summary, the results we have presented show that the breaking of angular ordering due to medium interactions has a more intricate behavior than previously known. While in this paper this was demonstrated in a simple setting, we look forward to extending our investigations to other phenomenologically relevant processes.

Acknowledgements

We are grateful to João Barata, Paul Caucal, Fabio Dominguez, Johannes Isaksen, Andrey Sadofyev, Carlos Salgado and Konrad Tywoniuk for insightful discussions during the development of this project. XML and GM thank the CERN theoretical department for the hospitality at different stages of this work. The work of XML and GM is supported by European Research Council project ERC-2018-ADG-835105 YoctoLHC. XML contribution to this work is also supported Xunta de Galicia (Centro singular de investigación de Galicia accreditation 2019-2022), by European Union ERDF; and by Grant CEX2023- 001318-M funded by MICIU/AEI/10.13039/501100011033 and by ERDF/EU, and under scholarship

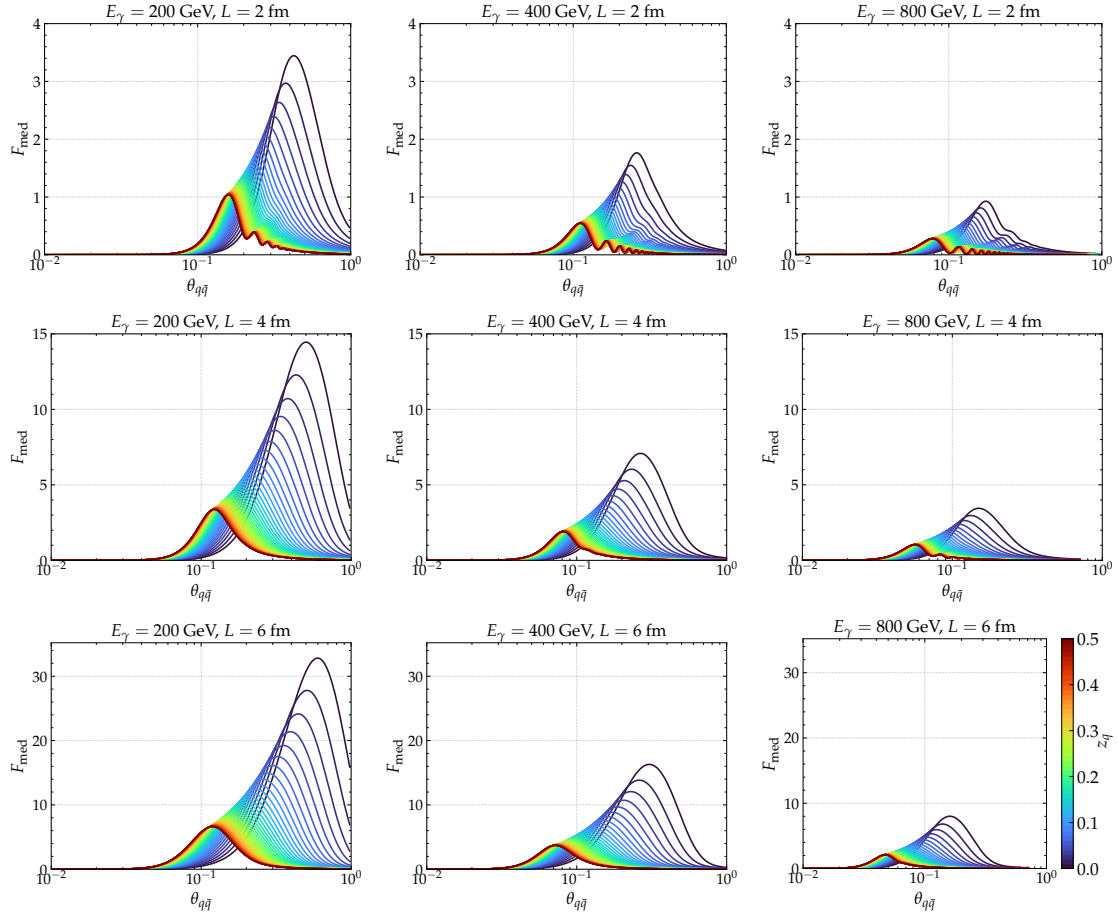


Figure 7: Numerical evaluation of F_{med} , Eq. (3.27), as a function of the opening angle of the antenna, $\theta_{q\bar{q}}$, and the energy sharing fraction, z_q , for different photon energies and medium lengths. Note the different limits on the y -axis for each row.

No. PRE2021-097748, funded by MCIN/AEI/10.13039/501100011033 and FSE+. ASO is supported by the Ramón y Cajal program under grant RYC2022-037846-I.

A Complementary material

In this appendix we collect some numerical results that complement those presented in the main text.

Figure 7 shows the behaviour of F_{med} in the parameter space described in the main text. This function controls both the total rate of emissions (see Eq. (3.31)) and the denominator of $\tilde{\Delta}_{\text{med}}$ (see Eq.(3.30)). In contrast to $\tilde{\Delta}_{\text{med}}$, we note that F_{med} is not bounded by one and it grows when decreasing E_γ or, equivalently, when increasing the antenna formation time. This implies a stronger medium modification of the spectrum for long antenna formation times, as expected. Something that has not been discussed previously in the literature are the oscillations that we observe for $L = 2$ fm and for $L = 4$ fm when setting $E_\gamma = 800$ GeV. One could argue that the former is outside the regime

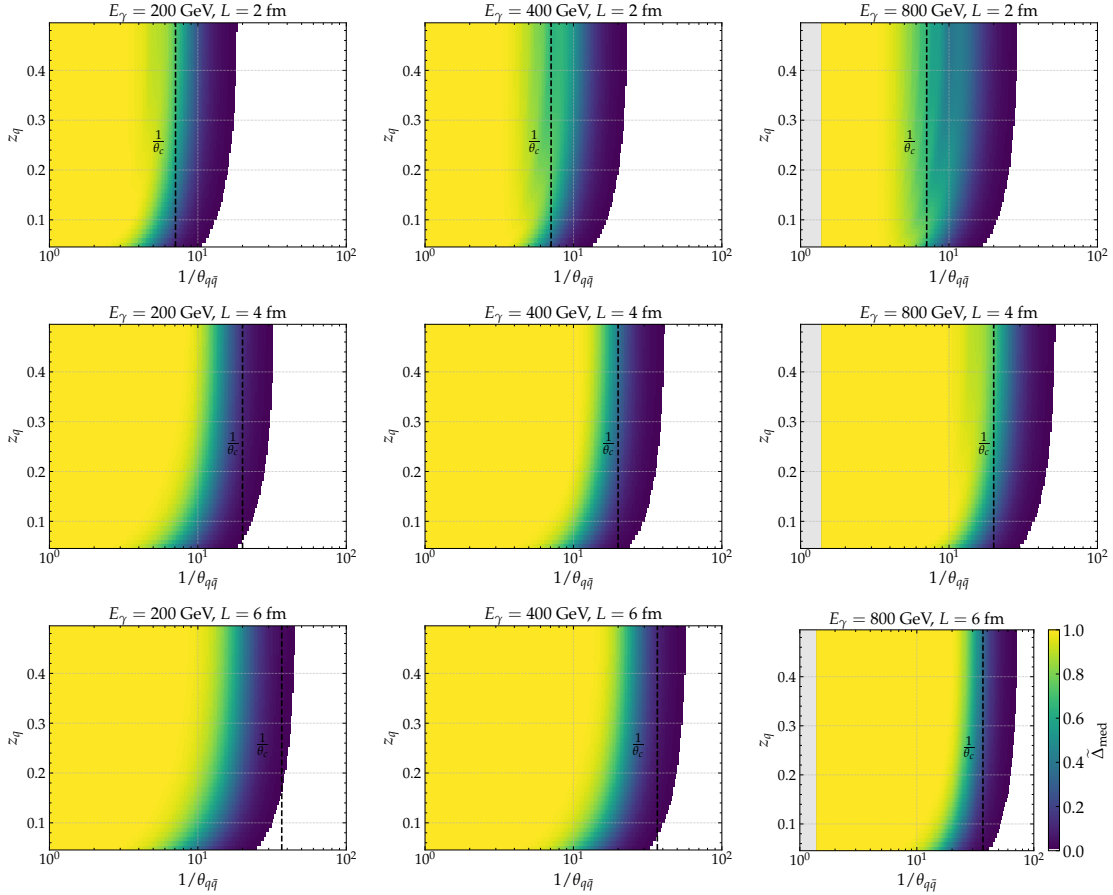


Figure 8: Lund plane representation of the generalized decoherence factor $\tilde{\Delta}_{\text{med}}$ for different medium lengths and photon energies. The gray band delineates the regime where we found numerical instabilities. The vertical dashed line indicates the position of θ_c , i.e., the value at which $\Delta_{\text{med}} = 1 - e^{-1}$.

of validity of our approximations, since the medium is too dilute. The latter, however, is consistent with them. As discussed in the main text, the origin of these oscillations is an interplay between the frequency of the trigonometric functions when increasing E_γ , and the slower exponential decay of the Wilson-line correlators when decreasing $\hat{q}L$. Furthermore, we have verified that these oscillations are not an artifact of the numerical integration (see footnote 6). Regarding the asymptotic behavior of F_{med} , we find that collinear splittings remain vacuum-like ($F_{\text{med}} = 0$) for all values of z_q . In the large-angle regime, emissions with $z_q \sim 0.5$ are also vacuum-like. The small- z_q curves do not vanish at wide-angles but, as we have already mentioned before, this part of the phase-space is beyond the regime of validity of our approximations and so these observations should be taken with care.

Finally, we show in Fig. 8 a Lund plane representation of $\tilde{\Delta}_{\text{med}}$ for the parameter space explored in this work. This provides a more visual way of identifying the regions of phase-space for which certain phenomena take place. For example, the regime of total colour decoherence is clearly visible when $\theta_{q\bar{q}} \rightarrow 1$ for any value of z_q . When the antenna is

sufficiently collinear, $\tilde{\Delta}_{\text{med}}$ vanishes and no anti-angular ordered emissions take place. For moderate angles, we observe a strong dependence of $\tilde{\Delta}_{\text{med}}$ on both medium parameters and the photon energy, as discussed in the main text. In particular, focusing on the $E_\gamma = 400$ column we note how the region where $\tilde{\Delta}_{\text{med}} \rightarrow 1$ moves towards smaller angles when increasing $\hat{q}L$, thus indicating a stronger modification of the antenna emission pattern when considering denser media.

References

- [1] A. Majumder, M. Van Leeuwen, The Theory and Phenomenology of Perturbative QCD Based Jet Quenching, *Prog. Part. Nucl. Phys.* 66 (2011) 41–92. [arXiv:1002.2206](#), [doi:10.1016/j.pnpnp.2010.09.001](#).
- [2] Y. Mehtar-Tani, J. G. Milhano, K. Tywoniuk, Jet physics in heavy-ion collisions, *Int. J. Mod. Phys. A* 28 (2013) 1340013. [arXiv:1302.2579](#), [doi:10.1142/S0217751X13400137](#).
- [3] J.-P. Blaizot, Y. Mehtar-Tani, Jet Structure in Heavy Ion Collisions, *Int. J. Mod. Phys. E* 24 (11) (2015) 1530012. [arXiv:1503.05958](#), [doi:10.1142/S021830131530012X](#).
- [4] M. Connors, C. Nattrass, R. Reed, S. Salur, Jet measurements in heavy ion physics, *Rev. Mod. Phys.* 90 (2018) 025005. [arXiv:1705.01974](#), [doi:10.1103/RevModPhys.90.025005](#).
- [5] L. Cunqueiro, A. M. Sickles, Studying the QGP with Jets at the LHC and RHIC, *Prog. Part. Nucl. Phys.* 124 (2022) 103940. [arXiv:2110.14490](#), [doi:10.1016/j.pnpnp.2022.103940](#).
- [6] L. Apolinário, Y.-J. Lee, M. Winn, Heavy quarks and jets as probes of the QGP, *Prog. Part. Nucl. Phys.* 127 (2022) 103990. [arXiv:2203.16352](#), [doi:10.1016/j.pnpnp.2022.103990](#).
- [7] L. Apolinário, Y.-T. Chien, L. Cunqueiro Mendez, Jet substructure, *Int. J. Mod. Phys. E* 33 (07) (2024) 2430003. [doi:10.1142/S0218301324300030](#).
- [8] G. Aad, et al., Measurement of the jet radius and transverse momentum dependence of inclusive jet suppression in lead-lead collisions at $\sqrt{s_{NN}} = 2.76$ TeV with the ATLAS detector, *Phys. Lett. B* 719 (2013) 220–241. [arXiv:1208.1967](#), [doi:10.1016/j.physletb.2013.01.024](#).
- [9] J. Adam, et al., Measurement of inclusive charged-particle jet production in Au + Au collisions at $\sqrt{s_{NN}} = 200$ GeV, *Phys. Rev. C* 102 (5) (2020) 054913. [arXiv:2006.00582](#), [doi:10.1103/PhysRevC.102.054913](#).
- [10] A. M. Sirunyan, et al., First measurement of large area jet transverse momentum spectra in heavy-ion collisions, *JHEP* 05 (2021) 284. [arXiv:2102.13080](#), [doi:10.1007/JHEP05\(2021\)284](#).
- [11] S. Acharya, et al., Measurement of the radius dependence of charged-particle jet suppression in Pb–Pb collisions at $s_{NN} = 5.02$ TeV, *Phys. Lett. B* 849 (2024) 138412. [arXiv:2303.00592](#), [doi:10.1016/j.physletb.2023.138412](#).
- [12] R. Baier, Y. L. Dokshitzer, A. H. Mueller, S. Peigne, D. Schiff, Radiative energy loss of high-energy quarks and gluons in a finite volume quark - gluon plasma, *Nucl. Phys. B* 483 (1997) 291–320. [arXiv:hep-ph/9607355](#), [doi:10.1016/S0550-3213\(96\)00553-6](#).
- [13] B. G. Zakharov, Fully quantum treatment of the Landau-Pomeranchuk-Migdal effect in QED and QCD, *JETP Lett.* 63 (1996) 952–957. [arXiv:hep-ph/9607440](#), [doi:10.1134/1.567126](#).

- [14] M. Gyulassy, P. Levai, I. Vitev, Jet quenching in thin quark gluon plasmas. 1. Formalism, Nucl. Phys. B571 (2000) 197–233. [arXiv:hep-ph/9907461](#), [doi:10.1016/S0550-3213\(99\)00713-0](#).
- [15] U. A. Wiedemann, Gluon radiation off hard quarks in a nuclear environment: Opacity expansion, Nucl. Phys. B 588 (2000) 303–344. [arXiv:hep-ph/0005129](#), [doi:10.1016/S0550-3213\(00\)00457-0](#).
- [16] J. Casalderrey-Solana, J. G. Milhano, U. A. Wiedemann, Jet Quenching via Jet Collimation, J. Phys. G 38 (2011) 035006. [arXiv:1012.0745](#), [doi:10.1088/0954-3899/38/3/035006](#).
- [17] Y. L. Dokshitzer, V. S. Fadin, V. A. Khoze, Coherent Effects in the Perturbative QCD Parton Jets, Phys. Lett. B 115 (1982) 242–246. [doi:10.1016/0370-2693\(82\)90654-2](#).
- [18] B. R. Webber, A QCD Model for Jet Fragmentation Including Soft Gluon Interference, Nucl. Phys. B 238 (1984) 492–528. [doi:10.1016/0550-3213\(84\)90333-X](#).
- [19] G. Marchesini, B. R. Webber, Monte Carlo Simulation of General Hard Processes with Coherent QCD Radiation, Nucl. Phys. B 310 (1988) 461–526. [doi:10.1016/0550-3213\(88\)90089-2](#).
- [20] Y. L. Dokshitzer, V. A. Khoze, S. I. Troian, A. H. Mueller, QCD Coherence in High-Energy Reactions, Rev. Mod. Phys. 60 (1988) 373. [doi:10.1103/RevModPhys.60.373](#).
- [21] Y. L. Dokshitzer, V. A. Khoze, A. H. Mueller, S. I. Troian, Basics of perturbative QCD, 1991.
- [22] R. K. Ellis, W. J. Stirling, B. R. Webber, QCD and collider physics, Vol. 8, Cambridge University Press, 2011. [doi:10.1017/CB09780511628788](#).
- [23] Y. Mehtar-Tani, C. A. Salgado, K. Tywoniuk, Anti-angular ordering of gluon radiation in QCD media, Phys. Rev. Lett. 106 (2011) 122002. [arXiv:1009.2965](#), [doi:10.1103/PhysRevLett.106.122002](#).
- [24] Y. Mehtar-Tani, C. A. Salgado, K. Tywoniuk, Jets in QCD Media: From Color Coherence to Decoherence, Phys. Lett. B 707 (2012) 156–159. [arXiv:1102.4317](#), [doi:10.1016/j.physletb.2011.12.042](#).
- [25] J. Casalderrey-Solana, E. Iancu, Interference effects in medium-induced gluon radiation, JHEP 08 (2011) 015. [arXiv:1105.1760](#), [doi:10.1007/JHEP08\(2011\)015](#).
- [26] Y. Mehtar-Tani, K. Tywoniuk, Jet coherence in QCD media: the antenna radiation spectrum, JHEP 01 (2013) 031. [arXiv:1105.1346](#), [doi:10.1007/JHEP01\(2013\)031](#).
- [27] Y. Mehtar-Tani, C. A. Salgado, K. Tywoniuk, The radiation pattern of a QCD antenna in a dilute medium, JHEP 04 (2012) 064. [arXiv:1112.5031](#), [doi:10.1007/JHEP04\(2012\)064](#).
- [28] N. Armesto, H. Ma, Y. Mehtar-Tani, C. A. Salgado, K. Tywoniuk, Coherence effects and broadening in medium-induced QCD radiation off a massive $q\bar{q}$ antenna, JHEP 01 (2012) 109. [arXiv:1110.4343](#), [doi:10.1007/JHEP01\(2012\)109](#).
- [29] Y. Mehtar-Tani, C. A. Salgado, K. Tywoniuk, The Radiation pattern of a QCD antenna in a dense medium, JHEP 10 (2012) 197. [arXiv:1205.5739](#), [doi:10.1007/JHEP10\(2012\)197](#).
- [30] J. Casalderrey-Solana, Y. Mehtar-Tani, C. A. Salgado, K. Tywoniuk, New picture of jet quenching dictated by color coherence, Phys. Lett. B 725 (2013) 357–360. [arXiv:1210.7765](#), [doi:10.1016/j.physletb.2013.07.046](#).
- [31] M. R. Calvo, M. R. Moldes, C. A. Salgado, Color coherence in a heavy quark antenna

- radiating gluons inside a QCD medium, *Phys. Lett. B* 738 (2014) 448–452.
[arXiv:1403.4892](#), [doi:10.1016/j.physletb.2014.10.010](#).
- [32] F. Domínguez, J. G. Milhano, C. A. Salgado, K. Tywoniuk, V. Vila, Mapping collinear in-medium parton splittings, *Eur. Phys. J. C* 80 (1) (2020) 11. [arXiv:1907.03653](#),
[doi:10.1140/epjc/s10052-019-7563-0](#).
- [33] J. H. Isaksen, K. Tywoniuk, Precise description of medium-induced emissions, *JHEP* 09 (2023) 049. [arXiv:2303.12119](#), [doi:10.1007/JHEP09\(2023\)049](#).
- [34] P. Caucal, E. Iancu, A. H. Mueller, G. Soyez, Vacuum-like jet fragmentation in a dense QCD medium, *Phys. Rev. Lett.* 120 (2018) 232001. [arXiv:1801.09703](#),
[doi:10.1103/PhysRevLett.120.232001](#).
- [35] L. D. McLerran, R. Venugopalan, Computing quark and gluon distribution functions for very large nuclei, *Phys. Rev. D* 49 (1994) 2233–2241. [arXiv:hep-ph/9309289](#),
[doi:10.1103/PhysRevD.49.2233](#).
- [36] M. Gyulassy, X.-n. Wang, Multiple collisions and induced gluon Bremsstrahlung in QCD, *Nucl. Phys. B* 420 (1994) 583–614. [arXiv:nucl-th/9306003](#),
[doi:10.1016/0550-3213\(94\)90079-5](#).
- [37] A. V. Sadofyev, M. D. Sievert, I. Vitev, Ab initio coupling of jets to collective flow in the opacity expansion approach, *Phys. Rev. D* 104 (9) (2021) 094044. [arXiv:2104.09513](#),
[doi:10.1103/PhysRevD.104.094044](#).
- [38] S. Hauksson, S. Jeon, C. Gale, Momentum broadening of energetic partons in an anisotropic plasma, *Phys. Rev. C* 105 (1) (2022) 014914. [arXiv:2109.04575](#),
[doi:10.1103/PhysRevC.105.014914](#).
- [39] L. Antiporda, J. Bahder, H. Rahman, M. D. Sievert, Jet drift and collective flow in heavy-ion collisions, *Phys. Rev. D* 105 (5) (2022) 054025. [arXiv:2110.03590](#),
[doi:10.1103/PhysRevD.105.054025](#).
- [40] J. Barata, A. V. Sadofyev, C. A. Salgado, Jet broadening in dense inhomogeneous matter, *Phys. Rev. D* 105 (11) (2022) 114010. [arXiv:2202.08847](#),
[doi:10.1103/PhysRevD.105.114010](#).
- [41] C. Andres, F. Dominguez, A. V. Sadofyev, C. A. Salgado, Jet broadening in flowing matter: Resummation, *Phys. Rev. D* 106 (7) (2022) 074023. [arXiv:2207.07141](#),
[doi:10.1103/PhysRevD.106.074023](#).
- [42] Y. Fu, J. Casalderrey-Solana, X.-N. Wang, Asymmetric transverse momentum broadening in an inhomogeneous medium, *Phys. Rev. D* 107 (5) (2023) 054038. [arXiv:2204.05323](#),
[doi:10.1103/PhysRevD.107.054038](#).
- [43] J. a. Barata, X. Mayo López, A. V. Sadofyev, C. A. Salgado, Medium induced gluon spectrum in dense inhomogeneous matter, *Phys. Rev. D* 108 (3) (2023) 034018.
[arXiv:2304.03712](#), [doi:10.1103/PhysRevD.108.034018](#).
- [44] J. a. Barata, J. G. Milhano, A. V. Sadofyev, Picturing QCD jets in anisotropic matter: from jet shapes to energy energy correlators, *Eur. Phys. J. C* 84 (2) (2024) 174.
[arXiv:2308.01294](#), [doi:10.1140/epjc/s10052-024-12514-1](#).
- [45] M. V. Kuzmin, X. Mayo López, J. Reiten, A. V. Sadofyev, Jet quenching in anisotropic flowing matter, *Phys. Rev. D* 109 (1) (2024) 014036. [arXiv:2309.00683](#),
[doi:10.1103/PhysRevD.109.014036](#).

- [46] M. V. Kuzmin, X. Mayo López, Gluon radiation inside a flowing medium (6 2024). [arXiv:2406.14628](#).
- [47] Y. Mehtar-Tani, K. Tywoniuk, Radiative energy loss of neighboring subjects, Nucl. Phys. A 979 (2018) 165–203. [arXiv:1706.06047](#), [doi:10.1016/j.nuclphysa.2018.09.041](#).
- [48] J. a. Barata, C. A. Salgado, J. a. M. Silva, Gluon to $q\bar{q}$ antenna in anisotropic QCD matter: spin-polarized and azimuthal jet observables (7 2024). [arXiv:2407.04774](#).
- [49] T. Altinoluk, N. Armesto, G. Beuf, M. Martínez, C. A. Salgado, Next-to-eikonal corrections in the CGC: gluon production and spin asymmetries in pA collisions, JHEP 07 (2014) 068. [arXiv:1404.2219](#), [doi:10.1007/JHEP07\(2014\)068](#).
- [50] J. H. Isaksen, K. Tywoniuk, Wilson line correlators beyond the large- N_c , JHEP 21 (2020) 125. [arXiv:2107.02542](#), [doi:10.1007/JHEP11\(2021\)125](#).
- [51] J.-P. Blaizot, F. Dominguez, E. Iancu, Y. Mehtar-Tani, Medium-induced gluon branching, JHEP 01 (2013) 143. [arXiv:1209.4585](#), [doi:10.1007/JHEP01\(2013\)143](#).
- [52] L. Apolinário, N. Armesto, J. G. Milhano, C. A. Salgado, Medium-induced gluon radiation and colour decoherence beyond the soft approximation, JHEP 02 (2015) 119. [arXiv:1407.0599](#), [doi:10.1007/JHEP02\(2015\)119](#).
- [53] M. D. Sievert, I. Vitev, B. Yoon, A complete set of in-medium splitting functions to any order in opacity, Phys. Lett. B 795 (2019) 502–510. [arXiv:1903.06170](#), [doi:10.1016/j.physletb.2019.06.019](#).
- [54] Y. Mehtar-Tani, Relating the description of gluon production in pA collisions and parton energy loss in AA collisions, Phys. Rev. C 75 (2007) 034908. [arXiv:hep-ph/0606236](#), [doi:10.1103/PhysRevC.75.034908](#).
- [55] P. Caucal, E. Iancu, G. Soyez, Deciphering the z_g distribution in ultrarelativistic heavy ion collisions, JHEP 10 (2019) 273. [arXiv:1907.04866](#), [doi:10.1007/JHEP10\(2019\)273](#).
- [56] Y. Mehtar-Tani, D. Pablos, K. Tywoniuk, Cone-Size Dependence of Jet Suppression in Heavy-Ion Collisions, Phys. Rev. Lett. 127 (25) (2021) 252301. [arXiv:2101.01742](#), [doi:10.1103/PhysRevLett.127.252301](#).
- [57] C. Andres, F. Dominguez, R. Kunnawalkam Elayavalli, J. Holguin, C. Marquet, I. Moutl, Resolving the Scales of the Quark-Gluon Plasma with Energy Correlators, Phys. Rev. Lett. 130 (26) (2023) 262301. [arXiv:2209.11236](#), [doi:10.1103/PhysRevLett.130.262301](#).
- [58] M. Attems, J. Brewer, G. M. Innocenti, A. Mazeliauskas, S. Park, W. van der Schee, G. Soyez, U. A. Wiedemann, Medium-Enhanced cc^- Radiation, Phys. Rev. Lett. 132 (21) (2024) 212301. [arXiv:2209.13600](#), [doi:10.1103/PhysRevLett.132.212301](#).
- [59] A. M. Sirunyan, et al., Measurement of the Splitting Function in pp and Pb-Pb Collisions at $\sqrt{s_{NN}} = 5.02$ TeV, Phys. Rev. Lett. 120 (14) (2018) 142302. [arXiv:1708.09429](#), [doi:10.1103/PhysRevLett.120.142302](#).
- [60] G. Aad, et al., Measurement of substructure-dependent jet suppression in Pb+Pb collisions at 5.02 TeV with the ATLAS detector, Phys. Rev. C 107 (5) (2023) 054909. [arXiv:2211.11470](#), [doi:10.1103/PhysRevC.107.054909](#).
- [61] S. Acharya, et al., Measurement of the groomed jet radius and momentum splitting fraction in pp and Pb–Pb collisions at $\sqrt{s_{NN}} = 5.02$ TeV, Phys. Rev. Lett. 128 (10) (2022) 102001. [arXiv:2107.12984](#), [doi:10.1103/PhysRevLett.128.102001](#).

- [62] G. Aad, et al., Measurement of Suppression of Large-Radius Jets and Its Dependence on Substructure in Pb+Pb Collisions at sNN=5.02 TeV with the ATLAS Detector, *Phys. Rev. Lett.* 131 (17) (2023) 172301. [arXiv:2301.05606](#), [doi:10.1103/PhysRevLett.131.172301](#).
- [63] Z. Hulcher, D. Pablos, K. Rajagopal, Resolution Effects in the Hybrid Strong/Weak Coupling Model, *JHEP* 03 (2018) 010. [arXiv:1707.05245](#), [doi:10.1007/JHEP03\(2018\)010](#).
- [64] Y. Tachibana, et al., Hard jet substructure in a multistage approach, *Phys. Rev. C* 110 (4) (2024) 044907. [arXiv:2301.02485](#), [doi:10.1103/PhysRevC.110.044907](#).
- [65] P. Caucal, E. Iancu, A. H. Mueller, G. Soyez, Nuclear modification factors for jet fragmentation, *JHEP* 10 (2020) 204. [arXiv:2005.05852](#), [doi:10.1007/JHEP10\(2020\)204](#).
- [66] Y. Mehtar-Tani, K. Tywoniuk, Sudakov suppression of jets in QCD media, *Phys. Rev. D* 98 (5) (2018) 051501. [arXiv:1707.07361](#), [doi:10.1103/PhysRevD.98.051501](#).
- [67] J. Casalderrey-Solana, G. Milhano, D. Pablos, K. Rajagopal, Modification of Jet Substructure in Heavy Ion Collisions as a Probe of the Resolution Length of Quark-Gluon Plasma, *JHEP* 01 (2020) 044. [arXiv:1907.11248](#), [doi:10.1007/JHEP01\(2020\)044](#).
- [68] P. Caucal, A. Soto-Ontoso, A. Takacs, Dynamically groomed jet radius in heavy-ion collisions, *Phys. Rev. D* 105 (11) (2022) 114046. [arXiv:2111.14768](#), [doi:10.1103/PhysRevD.105.114046](#).
- [69] D. Pablos, A. Soto-Ontoso, Pushing forward jet substructure measurements in heavy-ion collisions, *Phys. Rev. D* 107 (9) (2023) 094003. [arXiv:2210.07901](#), [doi:10.1103/PhysRevD.107.094003](#).
- [70] L. Cunqueiro, D. Pablos, A. Soto-Ontoso, M. Spousta, A. Takacs, M. Verweij, Isolating perturbative QCD splittings in heavy-ion collisions, *Phys. Rev. D* 110 (1) (2024) 014015. [arXiv:2311.07643](#), [doi:10.1103/PhysRevD.110.014015](#).
- [71] Y. Mehtar-Tani, D. Pablos, K. Tywoniuk, Jet suppression and azimuthal anisotropy from RHIC to LHC, *Phys. Rev. D* 110 (1) (2024) 014009. [arXiv:2402.07869](#), [doi:10.1103/PhysRevD.110.014009](#).
- [72] J. a. Barata, F. Domínguez, C. A. Salgado, V. Vila, A modified in-medium evolution equation with color coherence, *JHEP* 05 (2021) 148. [arXiv:2101.12135](#), [doi:10.1007/JHEP05\(2021\)148](#).
- [73] L. Cunqueiro, D. Napoletano, A. Soto-Ontoso, Dead-cone searches in heavy-ion collisions using the jet tree, *Phys. Rev. D* 107 (9) (2023) 094008. [arXiv:2211.11789](#), [doi:10.1103/PhysRevD.107.094008](#).
- [74] C. Andres, F. Dominguez, J. Holguin, C. Marquet, I. Moul, Seeing beauty in the quark-gluon plasma with energy correlators, *Phys. Rev. D* 110 (3) (2024) L031503. [arXiv:2307.15110](#), [doi:10.1103/PhysRevD.110.L031503](#).
- [75] N. Armesto, C. A. Salgado, U. A. Wiedemann, Medium induced gluon radiation off massive quarks fills the dead cone, *Phys. Rev. D* 69 (2004) 114003. [arXiv:hep-ph/0312106](#), [doi:10.1103/PhysRevD.69.114003](#).
- [76] D. Pablos, S. Sanjurjo, Color Coherence Effects in Dipole-Quark Scattering in the Soft Limit (6 2024). [arXiv:2406.08550](#).
- [77] M. Fickinger, G. Ovanessian, I. Vitev, Angular distributions of higher order splitting functions in the vacuum and in dense QCD matter, *JHEP* 07 (2013) 059. [arXiv:1304.3497](#), [doi:10.1007/JHEP07\(2013\)059](#).

- [78] J. Casalderrey-Solana, D. Pablos, K. Tywoniuk, Two-gluon emission and interference in a thin QCD medium: insights into jet formation, JHEP 11 (2016) 174. [arXiv:1512.07561](#), [doi:10.1007/JHEP11\(2016\)174](#).
- [79] P. Arnold, S. Iqbal, The LPM effect in sequential bremsstrahlung, JHEP 04 (2015) 070, [Erratum: JHEP 09, 072 (2016)]. [arXiv:1501.04964](#), [doi:10.1007/JHEP09\(2016\)072](#).
- [80] P. Arnold, O. Elgedawy, S. Iqbal, Are Gluon Showers inside a Quark-Gluon Plasma Strongly Coupled? A Theorist's Test, Phys. Rev. Lett. 131 (16) (2023) 162302. [arXiv:2212.08086](#), [doi:10.1103/PhysRevLett.131.162302](#).
- [81] P. Arnold, O. Elgedawy, S. Iqbal, Landau-Pomeranchuk-Migdal effect in sequential bremsstrahlung: Gluon shower development, Phys. Rev. D 108 (7) (2023) 074015. [arXiv:2302.10215](#), [doi:10.1103/PhysRevD.108.074015](#).